

Ratio of kaon and pion leptonic decay constants

with $N_f = 2 + 1 + 1$ Wilson-clover twisted-mass fermions

C. Alexandrou,^{1,2} S. Bacchio,² G. Bergner,³ P. Dimopoulos,⁴ J. Finkenrath,²
R. Frezzotti,⁵ M. Garofalo,^{6,7} B. Kostrzewa,⁸ G. Koutsou,² P. Labus,⁹
F. Sanfilippo,¹⁰ S. Simula,¹⁰ M. Ueding,⁷ C. Urbach,⁷ and U. Wenger¹¹

¹*Department of Physics, University of Cyprus, 20537 Nicosia, Cyprus*

²*Computation-based Science and Technology Research Center, The Cyprus Institute,
20 Konstantinou Kavafi Street, 2121 Nicosia, Cyprus*

³*University of Jena, Institute for Theoretical
Physics, Max-Wien-Platz 1, D-07743 Jena, Germany*

⁴*Dipartimento di Scienze Matematiche, Fisiche e Informatiche,
Università di Parma and INFN, Gruppo Collegato di Parma,
Parco Area delle Scienze 7/a (Campus), I-43124 Parma Italy*

⁵*Dipartimento di Fisica, Università di Roma “Tor Vergata” and INFN, Sezione di Tor Vergata,
Via della Ricerca Scientifica 1, I-00133 Roma, Italy*

⁶*Dipartimento di Fisica, Università Roma Tre and INFN, Sezione di Roma Tre,
Via della Vasca Navale 84, I-00146 Rome, Italy*

⁷*HISKP (Theory), Rheinische Friedrich-Wilhelms-Universität Bonn,
Nussallee 14-16, 53115 Bonn, Germany*

⁸*High Performance Computing and Analytics Lab,
Rheinische Friedrich-Wilhelms-Universität Bonn,
Friedrich-Hirzebruch-Allee 8, 53115 Bonn, Germany*

⁹*Fraunhofer Institute for Industrial Mathematics (ITWM),
Fraunhofer-Platz 1, 67663 Kaiserslautern, Germany*

¹⁰*Istituto Nazionale di Fisica Nucleare, Sezione di Roma Tre,
Via della Vasca Navale 84, I-00146 Rome, Italy*

¹¹*Institute for Theoretical Physics, Albert Einstein Center for Fundamental Physics,
University of Bern, Sidlerstrasse 5, CH-3012 Bern, Switzerland*



We present a determination of the ratio of kaon and pion leptonic decay constants in isosymmetric QCD (isoQCD), f_K/f_π , making use of the gauge ensembles produced by the Extended Twisted Mass Collaboration (ETMC) with $N_f = 2 + 1 + 1$ flavors of Wilson-clover twisted-mass quarks, including configurations close to the physical point for all dynamical flavors. The simulations are carried out at three values of the lattice spacing ranging from ~ 0.068 to ~ 0.092 fm with linear lattice size up to $L \sim 5.5$ fm. The scale is set by the PDG value of the pion decay constant, $f_\pi^{isoQCD} = 130.4$ (2) MeV, at the isoQCD pion point, $M_\pi^{isoQCD} = 135.0$ (2) MeV, obtaining for the gradient-flow (GF) scales the values $w_0 = 0.17383$ (63) fm, $\sqrt{t_0} = 0.14436$ (61) fm and $t_0/w_0 = 0.11969$ (62) fm. The data are analyzed within the framework of SU(2) Chiral Perturbation Theory (ChPT) without resorting to the use of renormalized quark masses. At the isoQCD kaon point $M_K^{isoQCD} = 494.2$ (4) MeV we get $(f_K/f_\pi)^{isoQCD} = 1.1995$ (44), where the error includes both statistical and systematic uncertainties. Implications for the Cabibbo-Kobayashi-Maskawa (CKM) matrix element $|V_{us}|$ and for the first-row CKM unitarity are discussed.

I. INTRODUCTION

The leptonic decay constants of charged pseudoscalar (P) mesons are the crucial hadronic ingredients necessary for obtaining precise information on the Cabibbo-Kobayashi-Maskawa (CKM) matrix elements describing the weak mixings among quark flavors [1, 2]. Within the Standard Model (SM) the unitarity of the CKM matrix imposes important constraints on various sums of squares of matrix elements and, therefore, any violation of such constraints would imply the presence of physics beyond the SM. The way the CKM entries can be determined is based on the knowledge of the experimental leptonic decay rates and of the corresponding theoretical calculations. In particular, both the charged kaon and pion leptonic decay widths into muons are known experimentally with a good precision [3], obtaining for their ratio the value

$$\frac{\Gamma(K \rightarrow \mu\nu_\mu[\gamma])}{\Gamma(\pi \rightarrow \mu\nu_\mu[\gamma])} = 1.3367 (2)_\pi (29)_K [29] , \quad (1)$$

where $[\gamma]$ stands for the contribution of virtual and real photons. On the theoretical side, within the SM the above ratio is given by

$$\frac{\Gamma(K \rightarrow \mu\nu_\mu[\gamma])}{\Gamma(\pi \rightarrow \mu\nu_\mu[\gamma])} = \left| \frac{V_{us} f_K}{V_{ud} f_\pi} \right|^2 \frac{M_\pi^3}{M_K^3} \left(\frac{M_K^2 - m_\mu^2}{M_\pi^2 - m_\mu^2} \right)^2 (1 + \delta R_{K\pi}) , \quad (2)$$

where V_{ud} and V_{us} are the relevant CKM entries, $M_{\pi(K)}$ is the charged pion(kaon) mass, m_μ is the muon mass and $\delta R_{K\pi}$ represents the isospin breaking (IB) corrections due both to the mass difference ($m_d - m_u$) between the light u - and d -quarks and to the quark electric charges. Finally, in Eq. (2) f_K/f_π is the ratio of kaon and pion leptonic decay constants defined in isosymmetric QCD (isoQCD), i.e. with $m_u = m_d$ and zero quark electric charges.

Recently [4, 5] the IB correction $\delta R_{K\pi}$ has been determined using a non-perturbative approach, based on first principles, through QCD+QED simulations on the lattice, obtaining $\delta R_{K\pi} = -0.0126 (14)$. From Eq. (1) one has

$$\left| \frac{V_{us}}{V_{ud}} \right| \frac{f_K}{f_\pi} = 0.27683 (29)_{\text{exp}} (20)_{\text{th}} = 0.27683 (35) , \quad (3)$$

which corresponds to an accuracy of $\simeq 0.13\%$. As well known [6], the IB correction $\delta R_{K\pi}$ and the isoQCD ratio f_K/f_π separately depend on the prescription used to define what is meant by isoQCD, while only the product $(f_K/f_\pi)\sqrt{1 + \delta R_{K\pi}}$ is independent on such prescription. The hadronic prescription adopted in Refs. [4, 5] corresponds to

$$M_\pi^{isoQCD} = 135.0 \text{ (2) MeV} , \quad (4)$$

$$M_K^{isoQCD} = 494.2 \text{ (4) MeV} , \quad (5)$$

$$f_\pi^{isoQCD} = 130.4 \text{ (2) MeV} , \quad (6)$$

while the quantity $(m_d - m_u)$ is obtained from the difference between the experimental charged and neutral kaon masses. The physical pion and kaon masses (4-5) are consistent with those recommended by FLAG-3 [7], and the pion decay constant (6), derived according to Ref. [8] adopting the value of the CKM entry $|V_{ud}|$ from Ref. [9], is used to set the lattice scale¹.

In this work we present our determination of the leptonic decay constant ratio f_K/f_π at the physical isoQCD point given by Eqs. (4-6), evaluated using the ETMC gauge ensembles produced with $N_f = 2 + 1 + 1$ flavors of Wilson Clover twisted-mass quarks, including configurations close to the physical point for all dynamical flavors [11, 12]. The lattice data will be analyzed within the framework of SU(2) Chiral Perturbation Theory (ChPT) without making use of renormalized quark masses². By means of the pion data we determine the gradient-flow (GF) scales w_0 [13], $\sqrt{t_0}$ [14] and t_0/w_0 adopting the physical value (6) at the pion point (4) to set the lattice scale, obtaining

$$w_0 = 0.17383 \text{ (63) fm} , \quad (7)$$

$$\sqrt{t_0} = 0.14436 \text{ (61) fm} , \quad (8)$$

$$t_0/w_0 = 0.11969 \text{ (62) fm} , \quad (9)$$

¹ In Ref. [5] it has been shown that within the precision of the lattice simulations the prescription given by Eqs. (4-6) is equivalent to the Gasser-Rusetsky-Scimemi (GRS) scheme [10], where the renormalized quark masses and coupling constant in a given short-distance scheme (viz. the $\overline{\text{MS}}$ scheme) and at a given scale (viz. 2 GeV) are equal in the full QCD+QED and isoQCD theories. For completeness we mention that in the charm sector the D_s -meson mass $M_{D_s}^{isoQCD}$ was chosen to be equal to its experimental value $M_{D_s^\pm} = 1969.0 \text{ (1.4) MeV}$ [3].

² An analysis of the kaon and pion masses and decay constants in terms of renormalized quark masses is ongoing and will be presented in a forthcoming ETMC publication.

where the error includes both statistical and systematic uncertainties. Our findings (7-8) are a little larger than the MILC results [15] $w_0 = 0.1714_{-12}^{+15}$ fm and $\sqrt{t_0} = 0.1416_{-5}^{+8}$ fm as well as the HPQCD results [16] $w_0 = 0.1715$ (9) fm and $\sqrt{t_0} = 0.1420$ (8) fm, both obtained using the hadronic value (6) to set the lattice scale. Within $\simeq 1.5$ standard deviations our result (7) is consistent with the recent, precise BMW determination $w_0 = 0.17236$ (70) fm, obtained in Ref. [17] using the Ω^- -baryon mass to set the lattice scale. Furthermore, the differences with the recent results $w_0 = 0.1709(11)$ fm and $\sqrt{t_0} = 0.1422(14)$ fm, obtained in Ref. [18] using the Ω^- -baryon mass to set the lattice scale, are within ~ 2 and ~ 1.5 standard deviations, respectively.

As for the ratio f_K/f_π we determine its value at the physical isoQCD point (4-6) and in the continuum and infinite volume limits, obtaining

$$\left(\frac{f_K}{f_\pi}\right)^{isoQCD} = 1.1995 \quad (44) , \quad (10)$$

where again the error includes both statistical and systematic uncertainties.

The IB correction $\delta R_{K\pi} = -0.0126$ (14), determined in Refs. [4, 5] and adopted in Eqs. (2-3), stems from the sum of a QED and a strong IB terms, which are both prescription dependent as well as their sum and the isoQCD value (10). Within the GRS prescription (see footnote 1) they are equal respectively to -0.0062 (12) and -0.0064 (7). Thus, for the ratio of kaon and pion leptonic decay constant including strong IB effects (which we remind is prescription dependent) we get

$$\frac{f_{K^+}}{f_{\pi^+}} = 1.1957 \quad (44) . \quad (11)$$

For comparison, the $N_f = 2+1+1$ determinations, entering the FLAG-4 average [19], yield the value $(f_{K^+}^+/f_{\pi^+}^+) = 1.1932$ (19) [16, 20, 21], which is well consistent with our result (11). Once corrected for the strong IB effects obtained in Refs. [16, 20, 21], the FLAG-4 average becomes $(f_K/f_\pi)^{isoQCD} = 1.1966$ (18), which agrees with our finding (10).

Taking the updated value $|V_{ud}| = 0.97370$ (14) from super-allowed nuclear beta decays [3, 22], Eqs. (3) and (10) yield the following value for the CKM element $|V_{us}|$:

$$|V_{us}| = 0.22472 \quad (24)_{\text{exp}} \quad (84)_{\text{th}} = 0.22472 \quad (87) , \quad (12)$$

which is nicely consistent with the latest estimate $|V_{us}| = 0.2252$ (5) from leptonic modes provided by the PDG [3]. Correspondingly, using $|V_{ub}| = 0.00382$ (24) [3] the first-row CKM unitarity becomes

$$|V_{ud}|^2 + |V_{us}|^2 + |V_{ub}|^2 = 0.99861 \quad (48) , \quad (13)$$

which would imply a $\simeq 3\sigma$ tension with unitarity from leptonic modes.

The plan of the paper is as follows.

In Section II some details of the ETMC gauge ensembles and of the simulations are illustrated, while a more complete description is provided in Appendix A. For each gauge ensemble the pion mass and decay constant are extracted from the relevant two-point correlation functions using a single exponential fit in the appropriate regions of large time distances. Alternatively, in Appendix B the extraction of the ground-state properties is performed through the multiple exponential procedure of Ref. [23]. For one gauge ensemble (cA211.12.48), because of a small deviation from maximal twist, the mass and the decay constant are corrected as described in Appendix C. In Section III the SU(2) ChPT predictions at next-to-leading order (NLO) for the pion decay constant f_π , including finite volume effects (FVEs), are presented. For the ensembles cB211.25.XX, sharing the same light-quark mass and lattice spacing and differing only for the lattice size L , the FVEs are investigated using both the NLO and the resummed NNLO formulae of Ref. [24]. In Section IV, adopting the physical value (6) at the pion point (4), we perform two determinations of the GF scale w_0 using the data for either f_π or the quantity $X_\pi \equiv (f_\pi M_\pi^4)^{1/5}$, which is found to be less affected by statistical and systematic errors. The two determinations of w_0 agree very nicely, but the one based on the quantity X_π turns out to be more precise by a factor of ≈ 2.5 . In the same way the other two GF scales $\sqrt{t_0}$ and t_0/w_0 are determined in Appendix D, where our calculations of the relative GF scales w_0/a , $\sqrt{t_0}/a$ and $t_0/(w_0a)$ at the physical pion point are also described. In Section V we analyze the data for the decay constant ratio f_K/f_π using SU(2) ChPT. In Section VI the implications for V_{us} and the first-row CKM unitarity are discussed. Finally, our conclusions are collected in Section VII .

II. ETMC ENSEMBLES

In this work we make use of the gauge ensembles produced recently by ETMC in isoQCD with $N_f = 2 + 1 + 1$ flavors of Wilson-clover twisted-mass quarks and described in Refs. [11, 12]. The gluon action is the improved Iwasaki one [25], while the fermionic action includes a Clover term [26] with a coefficient fixed by its estimate in one-loop tadpole boosted perturbation theory [27]. Its inclusion turns out to be very beneficial for reducing cutoff effects, in particular on the neutral pion mass, thereby making numerically stable simulations close to the physical pion point [11].

The Wilson mass counterterms of the two degenerate light-quarks as well as of the strange and charm quarks are chosen in order to guarantee automatic $\mathcal{O}(a)$ -improvement [28, 29]. The masses of the strange and charm sea quarks are tuned to their physical values for each ensemble [11, 12]. For the valence strange and charm sectors, a mixed action setup employing Osterwalder-Seiler fermions [30], with the same critical mass as determined in the unitary setup, has been adopted in order to avoid any undesired strange-charm quark mixing (through cutoff effects) and to preserve the automatic $\mathcal{O}(a)$ -improvement of physical observables [31].

Some properties of the ETMC ensembles, which are relevant for this work, are collected in Table I, while the simulation setup is described in detail in Appendix A. With respect to Ref. [12] two other dedicated gauge ensembles, cB211.25.24 and cB211.25.32, have been produced for the investigation of finite volume effects (FVEs).

Note that in the case of the ensembles cB211.072.64 and cC211.06.80, corresponding respectively to a lattice spacing equal to $a \approx 0.082$ fm and $a \approx 0.069$ fm, the pion mass is simulated quite close to the physical isoQCD value (4).

For each ensemble we compute the pion correlator given by

$$C_\pi(t) = \frac{1}{L^3} \sum_{x,z} \langle 0 | P_5(x) P_5^\dagger(z) | 0 \rangle \delta_{t,(t_x-t_z)} , \quad (14)$$

where $P_5(x) = \bar{q}_\ell(x) \gamma_5 q_\ell(x)$ is a local interpolating pion field. The Wilson parameters of the two mass-degenerate valence quarks are always chosen to have opposite values. In

ensemble	β	V/a^4	a (fm)	$a\mu_\ell$	M_π (MeV)	L (fm)	$M_\pi L$	confs
cA211.53.24	1.726	$24^3 \times 48$	0.0947 (4)	0.00530	346.4 (1.6)	2.27	3.99	628
cA211.40.24		$24^3 \times 48$		0.00400	301.6 (2.1)	2.27	3.47	662
cA211.30.32		$32^3 \times 64$		0.00300	261.1 (1.1)	3.03	4.01	1237
cA211.12.48		$48^3 \times 96$		0.00120	167.1 (0.8)	4.55	3.85	322
cB211.25.24	1.778	$24^3 \times 48$	0.0816 (3)	0.00250	259.2 (3.0)	1.96	2.57	500
cB211.25.32		$32^3 \times 64$		0.00250	253.3 (1.4)	2.61	3.35	400
cB211.25.48		$48^3 \times 96$		0.00250	253.0 (1.0)	3.92	5.02	314
cB211.14.64		$64^3 \times 128$		0.00140	189.8 (0.7)	5.22	5.02	437
cB211.072.64		$64^3 \times 128$		0.00072	136.8 (0.6)	5.22	3.62	374
cC211.06.80	1.836	$80^3 \times 160$	0.0694 (3)	0.00060	134.2 (0.5)	5.55	3.78	401

TABLE I. Summary of the simulated light-quark bare mass, $a\mu_\ell = a\mu_u = a\mu_d$, of the pion mass M_π , of the lattice size L and of the product $M_\pi L$ for the various ETMC gauge ensembles used in this work. The values of the lattice spacing a in the fourth column, estimated in Appendix D 2 using the relative GF scale w_0/a of Table X, and the values of M_π and L in the sixth and seventh columns correspond to the absolute scale $w_0 = 0.17383$ (63) fm (see Eq. (7)). In the last column the number of gauge configurations analyzed for each ensemble is presented.

this way the squared pion mass differs from its continuum counterpart only by terms of $\mathcal{O}(a^2\mu_\ell)$ [28, 29].

At large time distances one has

$$C_\pi(t) \xrightarrow[t \gg a, (T-t) \gg a]{} \frac{\mathcal{Z}_\pi}{2M_\pi} \left[e^{-M_\pi t} + e^{-M_\pi(T-t)} \right], \quad (15)$$

so that the pion mass M_π and the matrix element $\mathcal{Z}_\pi = |\langle \pi | \bar{q}_\ell \gamma_5 q_\ell | 0 \rangle|^2$ can be extracted from the exponential fit given in the r.h.s. of Eq. (15).

For maximally twisted fermions the value of \mathcal{Z}_π determines the pion decay constant f_π without the need of the knowledge of any renormalization constant [28, 32], namely

$$af_\pi = 2a\mu_\ell \frac{\sqrt{a^4 \mathcal{Z}_\pi}}{aM_\pi \sinh(aM_\pi)}. \quad (16)$$

The time intervals $[t_{min}, t_{max}]$ adopted for the fit (15) of the pion correlation function (14) as well as the extracted values of the pion mass and decay constant in lattice units

are collected in Table II. As anticipated in the Introduction, in this work we will make also use of the data for the quantity X_π defined as

$$X_\pi \equiv (f_\pi M_\pi^4)^{1/5}, \quad (17)$$

which turns out to be less affected by lattice artifacts (see below Fig. 1 and later Section III C). The values of X_π in lattice units are shown in the last column of Table II. The statistical errors of the lattice data lie in the range $0.1 \div 1.1\%$ for the pion mass, in the range $0.2 \div 0.8\%$ for the pion decay constant and in the range $0.1 \div 0.9\%$ for the quantity X_π . We stress that in the case of the four ensembles cA211.12.48, cB211.14.64, cB211.072.64 and cC211.06.80 (which correspond to $M_\pi \lesssim 190$ MeV) the statistical errors of aX_π turn out to be less than half of those of af_π .

ensemble	β	V/a^4	$[t_{\min}/a, t_{\max}/a]$	aM_π	af_π	aX_π
cA211.53.24	1.726	$24^3 \times 48$	[13, 22]	0.16626 (51)	0.07106 (36)	0.14027 (41)
cA211.40.24		$24^3 \times 48$	[13, 22]	0.14477 (70)	0.06809 (30)	0.12450 (44)
cA211.30.32		$32^3 \times 64$	[13, 28]	0.12530 (16)	0.06674 (15)	0.11047 (12)
cA211.12.48		$48^3 \times 96$	[13, 40]	0.08022 (18)	0.06133 (33)	0.07621 (10)
cB211.25.24	1.778	$24^3 \times 48$	[14, 22]	0.10720 (118)	0.05355 (42)	0.09331 (79)
cB211.25.32		$32^3 \times 64$	[14, 28]	0.10475 (45)	0.05652 (38)	0.09259 (26)
cB211.25.48		$48^3 \times 96$	[14, 42]	0.10465 (14)	0.05726 (12)	0.09276 (10)
cB211.14.64		$64^3 \times 128$	[14, 56]	0.07848 (10)	0.05477 (12)	0.07303 (6)
cB211.072.64		$64^3 \times 128$	[14, 56]	0.05659 (8)	0.05267 (14)	0.05578 (5)
cC211.06.80	1.836	$80^3 \times 160$	[15, 70]	0.04720 (7)	0.04504 (10)	0.04676 (5)

TABLE II. *The time intervals $[t_{\min}, t_{\max}]$ adopted in the fit (15) of the pion correlation function (14) together with the extracted values of the pion mass M_π , the decay constant f_π and the quantity X_π , given by Eq. (17), in lattice units. Errors are statistical only.*

An alternative way to extract the pion mass and decay constant is the ODE procedure of Ref. [23]. The results obtained by applying this method to the pion correlation function (14) are collected in Appendix B and found to be totally consistent with the findings of the single exponential fit (15) of Table II.

In the case of the ensemble cA211.12.48 due to a small deviation from maximal twist a correction needs to be applied. According to Appendix C the squared pion mass is left uncorrected, while for the pion decay constant f_π we use the following formula

$$f_\pi|_{corrected} = f_\pi K_\ell , \quad (18)$$

where

$$K_\ell \equiv \sqrt{1 + (Z_A m_{PCAC}/\mu_\ell)^2} , \quad (19)$$

m_{PCAC} is the bare untwisted PCAC mass, Z_A is the renormalization constant of the axial current and μ_ℓ is the bare twisted mass of the light valence quarks. For the ensemble cA211.12.48 one has $Z_A \approx 0.75$ and $m_{PCAC}/\mu_\ell \simeq -0.21$ (5) [12].

The statistical accuracy of the correlator (14) is significantly improved by using the so-called ‘‘one-end’’ stochastic method [33], which includes spatial stochastic sources at a single time slice randomly chosen. Statistical errors are evaluated using the jackknife procedure.

The results obtained for the pion decay constant $w_0 f_\pi$ and for the quantity $w_0 X_\pi$ (see Eq. (17)), are shown in Fig. 1 for all the gauge ensembles. By comparing the results corresponding to the ensembles cB211.25.XX the FVEs are clearly visible in the case of f_π , while they are almost absent in the case of X_π . Moreover, also discretization effects in X_π turn out to be smaller than those present in f_π .

III. THE PION DECAY CONSTANT f_π WITHIN SU(2) CHPT

Within SU(2) ChPT [34] the pion decay constant f_π is given at NLO by

$$f_\pi = f [1 - 2\xi_\ell \log(\xi_\ell) + 2A_1 \xi_\ell] , \quad (20)$$

where

$$\xi_\ell \equiv \frac{2B m_\ell}{(4\pi f)^2} \quad (21)$$

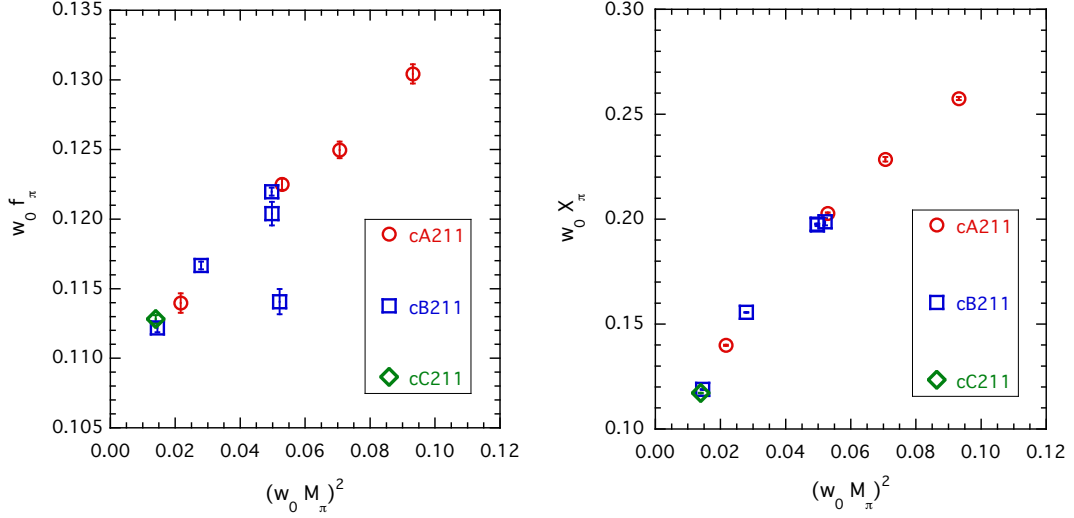


FIG. 1. Values of the pion decay constant $w_0 f_\pi$ (left panel) and of the quantity $w_0 X_\pi = w_0 (f_\pi M_\pi^4)^{1/5}$ (right panel) versus the squared pion mass $(w_0 M_\pi)^2$ in units of the GF scale w_0 . For the ensemble cA211.12.48 the corrected value of f_π given by Eq. (18) is considered.

with $m_\ell = m_u = m_d$ being the renormalized light-quark mass. In Eqs. (20-21) B and f are the LO SU(2) ChPT low-energy constants (LECs), while the coefficient A_1 is related to the NLO LEC $\bar{\ell}_4^{phys}$ by

$$\bar{\ell}_4^{phys} = A_1 + 2 \log \left(\frac{4\pi f}{M_\pi^{isoQCD}} \right). \quad (22)$$

For the squared pion mass one has at NLO

$$M_\pi^2 = 2Bm_\ell [1 + \xi_\ell \log(\xi_\ell) + C_1 \xi_\ell], \quad (23)$$

where the coefficient C_1 is related to the NLO LEC $\bar{\ell}_3^{phys}$ by

$$\bar{\ell}_3^{phys} = -C_1 + 2 \log \left(\frac{4\pi f}{M_\pi^{isoQCD}} \right). \quad (24)$$

A. Finite volume effects within NLO SU(2) ChPT

The structure of FVEs on the pion decay constant can be studied using SU(2) ChPT [34]. At NLO FVEs come entirely from the discretized sum over periodic momenta

of the loop contributions. For a finite spatial volume $V = L^3$ one has

$$f_\pi(L) = f_\pi(L \rightarrow \infty) [1 + \Delta_{FVE}^\pi(L)] , \quad (25)$$

where $f_\pi(L \rightarrow \infty)$ is given by Eq. (20). The correction term $\Delta_{FVE}^\pi(L)$ can be obtained from the chiral log in Eq. (20) via the following replacement

$$\xi_\ell \log(\xi_\ell) \rightarrow \xi_\ell \tilde{g}_1(\lambda) , \quad (26)$$

where $\lambda \equiv \sqrt{2Bm_\ell}L = \sqrt{\xi_\ell} 4\pi fL$ and

$$\tilde{g}_1(\lambda) = 4 \sum_{n=1}^{\infty} \frac{m(n)}{\sqrt{n}\lambda} K_1(\sqrt{n}\lambda) \quad (27)$$

with K_1 being a Bessel function of the second kind and $m(n)$ the multiplicities of a three-dimensional vector \vec{n} having integer norm n (i.e. $m(n) = \{6, 12, 8, 6, \dots\}$). At sufficiently large values of λ the Bessel function can be replaced by its asymptotic expansion, which leads to

$$\tilde{g}_1(\lambda) \simeq 4 \sqrt{\frac{\pi}{2}} \sum_{n=1}^{\infty} \frac{m(n)}{(\sqrt{n}\lambda)^{3/2}} e^{-\sqrt{n}\lambda} . \quad (28)$$

Thus, within NLO SU(2) ChPT the quantity $\Delta_{FVE}^\pi(L)$ is given by

$$\Delta_{FVE}^\pi(L) = -2\xi_\ell \tilde{g}_1(\lambda) . \quad (29)$$

In the case of the squared pion mass one gets

$$M_\pi^2(L) = M_\pi^2(L \rightarrow \infty) \left[1 - \frac{1}{4} \Delta_{FVE}^\pi(L) \right]^2 , \quad (30)$$

where $M_\pi^2(L \rightarrow \infty)$ is given by Eq. (23).

B. FVEs for the ensembles cB211.25.XX

In this Section we study the FVEs on the pion mass and decay constant corresponding to the three ensembles cB211.25.XX of Table I, which share the same light-quark mass and lattice spacing but differ only for the lattice size L . We consider SU(2) ChPT

both at NLO, i.e. the Gasser-Leutwyler (GL) formulae (25) and (30), and at NNLO + resummation, i.e. the Colangelo-Dürr-Haefeli (CDH) formulae [24]. The latter ones read as

$$f_\pi(L) = f_\pi(\infty) \left\{ 1 - 2\xi_\pi \tilde{g}_1(M_\pi L) + 2\xi_\pi^2 \left[C_{f_\pi}^{(1)} \tilde{g}_1(M_\pi L) + C_{f_\pi}^{(2)} \tilde{g}_2(M_\pi L) + S_{f_\pi}^{(4)} \right] \right\}, \quad (31)$$

$$M_\pi(L) = M_\pi(\infty) \left\{ 1 + \frac{1}{2} \xi_\pi \tilde{g}_1(M_\pi L) - \xi_\pi^2 \left[C_{M_\pi}^{(1)} \tilde{g}_1(M_\pi L) + C_{M_\pi}^{(2)} \tilde{g}_2(M_\pi L) + S_{M_\pi}^{(4)} \right] \right\}, \quad (32)$$

where \tilde{g}_1 is defined in Eq. (27), while

$$\tilde{g}_2(\lambda) \equiv 4 \sum_{n=1}^{\infty} \frac{m(n)}{\sqrt{n}\lambda} \frac{K_2(\sqrt{n}\lambda)}{\sqrt{n}\lambda} \quad (33)$$

and

$$C_{f_\pi}^{(1)} = -\frac{7}{9} + 2\bar{\ell}_1 + \frac{4}{3}\bar{\ell}_2 - 3\bar{\ell}_4, \quad (34)$$

$$C_{f_\pi}^{(2)} = \frac{112}{9} - \frac{8}{3}\bar{\ell}_1 - \frac{32}{3}\bar{\ell}_2, \quad (35)$$

$$C_{M_\pi}^{(1)} = -\frac{55}{18} + 4\bar{\ell}_1 + \frac{8}{3}\bar{\ell}_2 - \frac{5}{2}\bar{\ell}_3 - 2\bar{\ell}_4, \quad (36)$$

$$C_{M_\pi}^{(2)} = C_{f_\pi}^{(2)} = \frac{112}{9} - \frac{8}{3}\bar{\ell}_1 - \frac{32}{3}\bar{\ell}_2 \quad (37)$$

with $\bar{\ell}_i$ being NLO LECs that have a logarithmic pion mass dependence

$$\bar{\ell}_i = \bar{\ell}_i^{phys} + 2 \log \left(\frac{M_\pi^{isoQCD}}{M_\pi} \right). \quad (38)$$

Finally, in Eqs. (31)-(32) the NNLO terms $S_{f_\pi}^{(4)}$ and $S_{M_\pi}^{(4)}$ are defined in the Appendix A of Ref. [24], but useful approximate analytic formulae are given by [24]

$$S_{f_\pi}^{(4)} = \left(\frac{4}{3}s_0 - \frac{13}{6}s_1 \right) \tilde{g}_1(M_\pi L) - \left(\frac{40}{3}s_0 - 4s_1 - \frac{8}{3}s_2 - \frac{13}{3}s_3 \right) \tilde{g}_2(M_\pi L), \quad (39)$$

$$S_{M_\pi}^{(4)} = \frac{13}{3}s_0 \tilde{g}_1(M_\pi L) - \left(\frac{40}{3}s_0 + \frac{32}{3}s_1 + \frac{26}{3}s_2 \right) \tilde{g}_2(M_\pi L) \quad (40)$$

with

$$s_0 = 2 - \frac{\pi}{2}, \quad s_1 = \frac{\pi}{4} - \frac{1}{2}, \quad s_2 = \frac{1}{2} - \frac{\pi}{8}, \quad s_3 = \frac{3\pi}{16} - \frac{1}{2}. \quad (41)$$

The expansion variable ξ_π is defined as [24]

$$\xi_\pi \equiv \frac{M_\pi^2}{(4\pi f_\pi)^2} . \quad (42)$$

Different choices of the expansion variable are possible: one can replace f_π with the LO LEC f and/or replace M_π^2 with $2Bm_\ell$ (and correspondingly $M_\pi L$ with $\sqrt{2Bm_\ell}L$ in the arguments of the functions \tilde{g}_1 and \tilde{g}_2). At NLO (i.e., for the GL formula) the above changes are equivalent, since any difference represents a NNLO effect. Instead, in the CDH formula additional terms appear at NNLO, which can be found in Ref. [35]. Here we consider only the alternative definition

$$\xi_\pi \rightarrow \frac{M_\pi^2}{(4\pi f)^2} , \quad (43)$$

which requires the addition to the r.h.s of Eq. (31) of the term $f_\pi(\infty) \{8\xi_\pi^2 \bar{\ell}_4 \tilde{g}_1(M_\pi L)\}$ and to the r.h.s. of Eq. (32) of the term $M_\pi(\infty) \{-2\xi_\pi^2 \bar{\ell}_4 \tilde{g}_1(M_\pi L)\}$.

The GL formula corresponds to Eqs. (31)-(32) with all C 's and S 's set equal to zero. The CDH formula requires the knowledge of the values of the four NLO LECs $\bar{\ell}_i^{phys}$ with $i = 1, \dots, 4$.

In Figs. 2 and 3 we compare the FVEs on the pion mass and decay constant for the three ensembles cB211.25.XX of Table I, evaluated using the GL and CDH formulae and assuming respectively the two definitions (42) and (43) for the expansion variable ξ_π .

In the case of CDH formula we adopt the following values of the NLO LECs: $\bar{\ell}_1^{phys} = -0.4$, $\bar{\ell}_2^{phys} = 4.3$, $\bar{\ell}_3^{phys} = 3.2$ and $\bar{\ell}_4^{phys} = 4.4$ (see Ref. [35]). The CDH results depend on such a choice and the sensitivity to the specific value of $\bar{\ell}_2^{phys}$ is illustrated in both figures by the green triangles.

It can be seen that the GL formula applied to both the pion mass and decay constant works quite well for $M_\pi L \gtrsim 3$, particularly in the case of the definition (43) of the expansion variable ξ_π . The above condition is satisfied by all ETMC ensembles of Table I except the ensemble cB211.25.24.

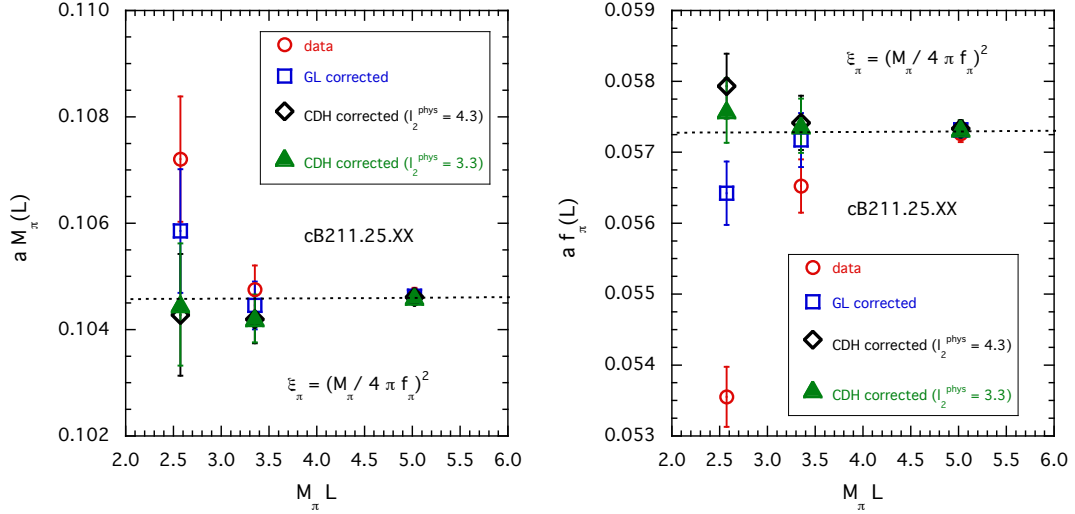


FIG. 2. Values of the pion mass (left panel) and pion decay constant (right panel) in lattice units for the three ensembles $cB211.25.XX$ of Table I. The red circles represent the data versus $M_\pi L$. The expansion variable ξ_π is given by Eq. (42). The blue squares correspond to the data corrected by the GL formula, while black diamonds represent the data corrected by the CDH formula, adopting for the NLO LECs the values $\bar{\ell}_1^{phys} = -0.4$, $\bar{\ell}_2^{phys} = 4.3$, $\bar{\ell}_3^{phys} = 3.2$ and $\bar{\ell}_4^{phys} = 4.4$. The green triangles correspond to the CDH correction assuming $\bar{\ell}_2^{phys} = 3.3$. The horizontal dotted lines are the values of the pion mass and decay constant in the infinite volume limit.

C. FVEs for the quantity X_π

The interesting feature of the quantity X_π , given by Eq. (17), is the absence of NLO chiral logs in its SU(2) ChPT expansion (see Eqs. (20) and (23)) when expressed in terms of quark masses. This implies the absence of FVEs at NLO, which in turn is also the origin of the small FVEs observed in the right panel of Fig. 1. This point is better elucidated in Fig. 4, where the results corresponding to the three ensembles $cB211.25.XX$ differing only in the lattice size L are shown.

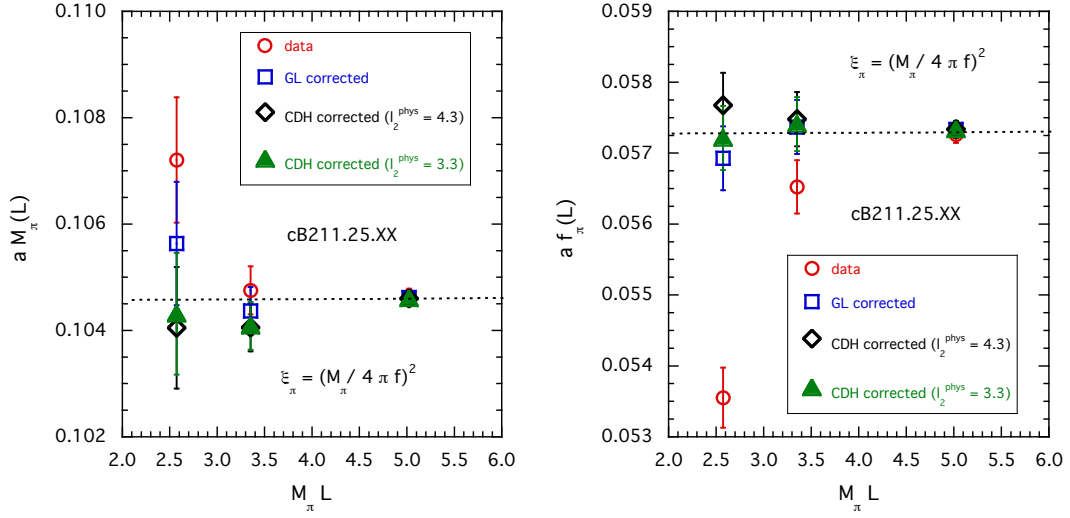


FIG. 3. The same as in Fig. 2, but adopting the alternative definition (43) for the expansion variable ξ_π and assuming $f = 122.5 \text{ MeV}$ and $a = 0.080 \text{ fm}$.

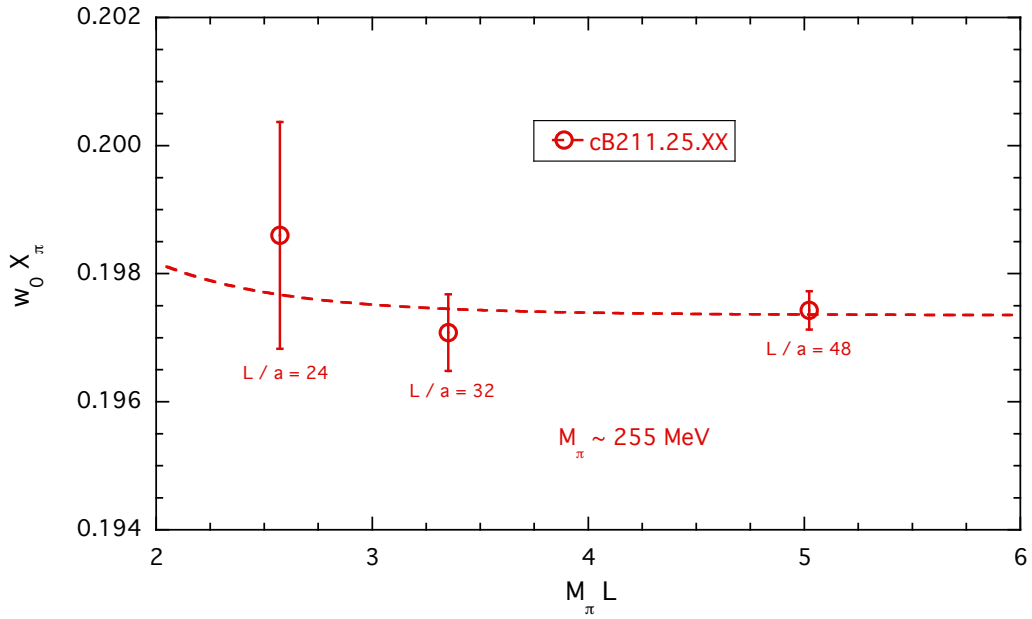


FIG. 4. Values of $w_0 X_\pi$ versus $M_\pi L$ for the three ensembles cB211.25.XX differing only for the lattice size L . The dashed line indicates the simple exponential fit of the form $A [1 + Be^{-M_\pi L} / (M_\pi L)^{3/2}]$.

IV. DETERMINATION OF THE GF SCALE w_0 FROM THE PION DATA

Let's now apply the SU(2) ChPT predictions for interpolating the pion data to the physical pion mass and for extrapolating them to the continuum and infinite volume limits. The goal is to determine the GF scale w_0 adopting the physical value (6) at the pion point (4) without resorting to the use of the renormalized light-quark mass. In the next two subsections we separately analyze the pion decay constant f_π and the quantity X_π , respectively.

A. Determination of w_0 using the data for f_π

Using the simulated values aM_π and af_π in lattice units we evaluate the expansion variable ξ_π , defined (from now on) as

$$\xi_\pi \equiv \frac{(aM_\pi)^2}{(4\pi af_\pi)^2} = \frac{M_\pi^2}{(4\pi f_\pi)^2}, \quad (44)$$

which depends on neither w_0 nor w_0/a . Then, for each gauge ensemble we calculate the FVE correction $\Delta_{FVE}^\pi(L)$ as

$$\Delta_{FVE}^\pi(L) = -2\xi_\pi \tilde{g}_1(M_\pi L) \quad (45)$$

and we re-express the quantity ξ_ℓ (see Eq. (21)) in terms of the pion mass in the infinite volume limit (see Eq. (30))

$$\xi_\ell \rightarrow \xi \equiv \frac{M_\pi^2(L \rightarrow \infty)}{(4\pi f)^2} = \frac{(w_0 M_\pi)^2}{(4\pi w_0 f)^2} \frac{1}{\left[1 - \frac{1}{4}\Delta_{FVE}^\pi(L)\right]^2}, \quad (46)$$

where only the knowledge of w_0/a is required to calculate the pion mass in units of w_0 and the free parameter becomes $w_0 f$.

We correct the data of the pion decay constant $w_0 f_\pi(L)$ for FVEs (see Eq. (25)), namely

$$w_0 f_\pi(L \rightarrow \infty) = \frac{w_0 f_\pi(L)}{1 + \Delta_{FVE}^\pi(L)}. \quad (47)$$

Analogously, for the pion mass $w_0 M_\pi(L)$ one has

$$w_0 M_\pi(L \rightarrow \infty) = \frac{w_0 M_\pi(L)}{1 - \frac{1}{4} \Delta_{FVE}^\pi(L)}. \quad (48)$$

The data for $w_0 f_\pi(L \rightarrow \infty)$ are fitted in terms of the variable ξ (see Eq. (46)) using the following functional form

$$w_0 f_\pi(L \rightarrow \infty) = w_0 f \left[1 - 2\xi \log(\xi) + 2A_1 \xi + A_2 \xi^2 + \frac{a^2}{w_0^2} (D_0 + D_1 \xi) \right] \quad (49)$$

where with respect to a pure NLO ansatz we have added a possible higher-order term quadratic in ξ as well as discretization effects proportional to a^2 and $a^2 M_\pi^2$.

The free parameters appearing in Eq. (49) are $w_0 f$, A_1 , A_2 , D_0 , D_1 and their values are obtained from a standard χ^2 -minimization. From the value of $w_0 f$ the GF scale w_0 can be determined as follows. Let us consider the physical value of the variable (44), namely

$$\xi_\pi^{isoQCD} \equiv \left[\frac{M_\pi^{isoQCD}}{4\pi f_\pi^{isoQCD}} \right]^2 = 0.006785 \quad (29). \quad (50)$$

Using Eq. (49) in the continuum limit the physical value of the variable (46), namely $\xi^{isoQCD} = (M_\pi^{isoQCD}/4\pi f)^2$, can be obtained by solving the relation

$$\xi_\pi^{isoQCD} = \frac{\xi^{isoQCD}}{[1 - 2\xi^{isoQCD} \log(\xi^{isoQCD}) + 2A_1 \xi^{isoQCD} + A_2 (\xi^{isoQCD})^2]^2}. \quad (51)$$

In this way the value of the LEC f in physical units is given by $f = M_\pi^{isoQCD}/(4\pi \sqrt{\xi^{isoQCD}})$ and, therefore, w_0 can be determined using the value of $w_0 f$.

We start by considering a pure NLO fit, i.e. $A_2 = 0$, including only the discretization effect proportional to a^2 , i.e. $D_1 = 0$ in Eq. (49), and we apply it to all pion data up to $M_\pi \simeq 350$ MeV. The discretization coefficient D_0 turns out to be quite small, $D_0 = -0.05(4)$, and the corresponding $\chi^2/(d.o.f.)$ is equal to $\chi^2/(d.o.f.) \simeq 1.5$ for 10 data points and 3 parameters. For the GF scale w_0 we get $w_0 = 0.1712(14)$ fm, which exhibits a $\simeq 0.8\%$ accuracy. However, a drastic improvement in the quality of the fit is obtained by including the discretization term proportional to $a^2 M_\pi^2$, i.e. $D_1 \neq 0$. This leads to $\chi^2/(d.o.f.) \simeq 0.2$, obtaining for w_0 the value

$$w_0 = 0.1740 \quad (15) \text{ fm} \quad (52)$$

with $f = 124.4(6)$ MeV and $\bar{\ell}_4^{phys} = 3.24(29)$ (see Eq. (22)). The quality of the above fit is illustrated in Fig. 5. The result (52) is confirmed by a NLO fit without the dis-

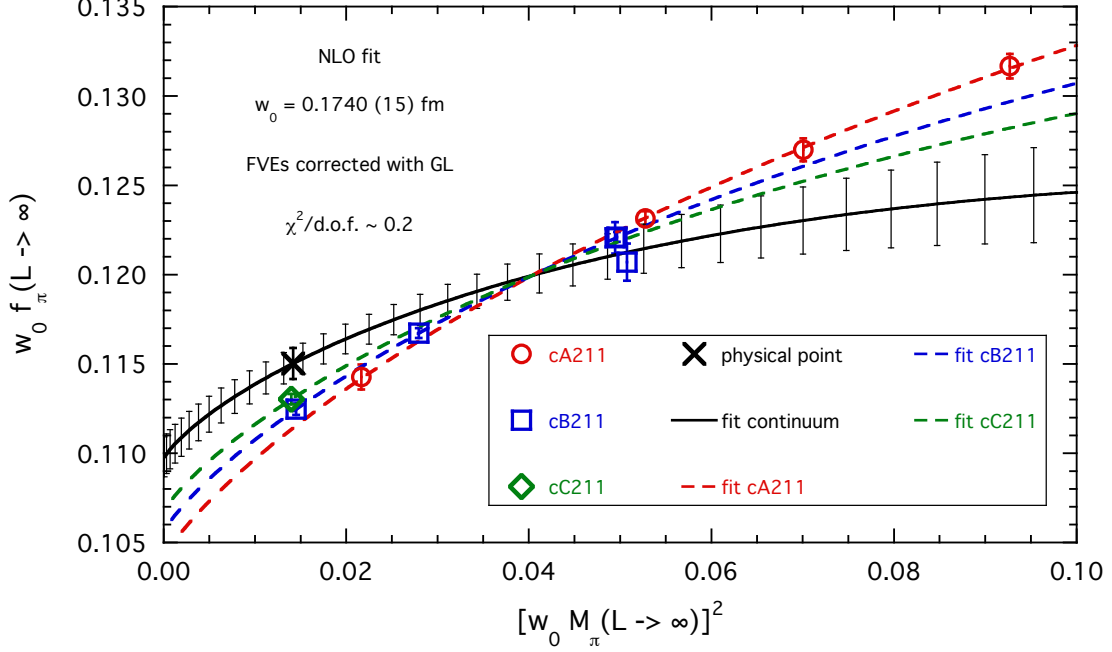


FIG. 5. Values of the pion decay constant $w_0 f_\pi$ corrected for FVEs according to Eq. (47) (open markers) and compared to the results of the NLO ChPT fit corresponding to $A_2 = 0$ in Eq. (49) applied to all data points ($M_\pi \lesssim 350$ MeV). The solid line represents the results of the fit in the continuum limit, while the dashed lines correspond to the fit evaluated at each value of β . The cross represents the result at the physical pion point (4) corresponding to the value $w_0 = 0.1740(15)$ fm, obtained as described in the text.

cretization effects proportional to $a^2 M_\pi^2$ (i.e. $D_1 = 0$), but limited to pion masses below $\simeq 190$ MeV (4 data points and 3 parameters). In this case one gets $w_0 = 0.1736(15)$ fm, $f = 122.8(4)$ MeV, $\bar{\ell}_4^{phys} = 4.06(18)$ and $\chi^2/(\text{d.o.f.}) \simeq 0.1$.

In order to investigate systematic effects we include the quadratic term proportional to A_2 , obtaining $w_0 = 0.1737(16)$ fm, $f = 124.3(7)$ MeV, $\bar{\ell}_4^{phys} = 3.26(30)$ and $\chi^2/(\text{d.o.f.}) \simeq 0.2$, and we check also the impact of FVEs by multiplying the correction $\Delta_{FVE}^\pi(L)$ of Eq. (45) by a factor κ_{FVE} used as a further free parameter in the NLO fit. The factor κ_{FVE} turns out to be consistent with unity, $\kappa_{FVE} = 1.20(18)$, and we

get $w_0 = 0.1743(16)$ fm, $f = 124.5(6)$ MeV, $\bar{\ell}_4^{phys} = 3.18(30)$ and $\chi^2/(\text{d.o.f.}) \simeq 0.1$.

After averaging the above results our determinations of w_0 , f and $\bar{\ell}_4^{phys}$ based on the analysis of f_π are

$$w_0 = 0.17390(157)_{stat+fit}(30)_{syst}[160] \text{ fm} , \quad (53)$$

$$f = 124.0(6)_{stat+fit}(7)_{syst}[9] \text{ MeV} , \quad (54)$$

$$\bar{\ell}_4^{phys} = 3.44(27)_{stat+fit}(36)_{syst}[45] , \quad (55)$$

where $()_{stat+fit}$ incorporates the uncertainties induced by both the statistical errors and the fitting procedure itself, $()_{syst}$ corresponds to the uncertainty related to chiral interpolation, discretization and finite-volume effects, while the last error is their sum in quadrature. More precisely, the various systematic uncertainties are estimated by considering the results obtained with $A_2 = 0$ or $A_2 \neq 0$ in the case of the chiral extrapolation, with $D_1 \neq 0$ or $D_1 = 0$ (but limited to $M_\pi < 190$ MeV) for the discretization effects and with $\kappa_{FVE} = 1$ or $\kappa_{FVE} \neq 1$ for the FVEs.

B. Determination of the GF scale w_0 using the data for X_π

In this Section we illustrate the results of the analysis of the lattice data for the quantity $w_0 X_\pi$ adopting the following fitting function

$$w_0 X_\pi = (w_0 f) \left\{ (4\pi)^4 \xi^2 \left[1 - 2\xi \log(\xi) + 2A_1 \xi + A_2' \xi^2 + a^2 (D_0' + D_1' \xi) \right] \right\}^{1/5} \cdot \left(1 + F_{FVE} \xi^2 e^{-M_\pi L} / (M_\pi L)^{3/2} \right) , \quad (56)$$

where the variable ξ is defined by Eq. (46), given in terms of the pion mass corrected for the FVEs using the GL formula (45), and the coefficient A_1 is related to the LEC $\bar{\ell}_4^{phys}$ by Eq. (22). In Eq. (56) we have taken into account that the FVEs on X_π start only at NNLO, i.e. at order $\mathcal{O}(\xi^2)$. Their impact is obtained by including ($F_{FVE} \neq 0$) or by excluding ($F_{FVE} = 0$) the higher order FVEs. Moreover, the NLO chiral log is present only because we employ meson masses and it would disappear if the light-quark mass

would be instead considered (in this case the linear coefficient A_1 provides directly the difference $\bar{\ell}_4^{phys} - \bar{\ell}_3^{phys}$).

We have performed several fits similar to those adopted in Section IV A and the corresponding results are collected in Table III. The quality of the NLO fit with $D'_1 \neq 0$

$A'_2 \neq 0$	$D'_1 \neq 0$	$F_{FVE} \neq 0$	range of M_π	w_0 (fm)	f (MeV)	$\bar{\ell}_4^{phys}$	$\chi^2/(d.o.f.)$
no	no	no	< 350 MeV	0.17213 (47)	122.4 (0.7)	4.23 (9)	0.26
no	yes	no	< 350 MeV	0.17394 (58)	124.4 (1.2)	3.24 (29)	0.03
no	no	no	< 190 MeV	0.17343 (53)	122.8 (1.0)	4.04 (16)	0.05
yes	yes	no	< 350 MeV	0.17378 (56)	124.3 (1.3)	3.27 (30)	0.04
no	yes	yes	< 350 MeV	0.17415 (61)	124.6 (1.3)	3.15 (35)	0.02

TABLE III. Results for w_0 obtained by fitting the lattice data for $w_0 X_\pi$ using Eq. (56) and adopting the isoQCD values (4) and (6) for fixing the lattice scale at the physical pion point.

is illustrated in Fig. 6, where it is also clearly visible the presence of discretization effects proportional to $a^2 M_\pi^2$, as already observed in the case of $w_0 f_\pi$ (see Fig. 5). We stress that for both quantities, $w_0 f_\pi$ and $w_0 X_\pi$, the inclusion of a discretization term proportional to $a^2 M_\pi^2$ leads to higher values of w_0 . This result is reassuringly confirmed also by a NLO fit without such a discretization term (i.e. $D'_1 = 0$), but limited to pion masses below $\simeq 190$ MeV (see the fourth row of Table III).

By averaging the last four results of Table III one has

$$w_0 = 0.17383 (57)_{\text{stat+fit}} (26)_{\text{syst}} [63] \text{ fm} , \quad (57)$$

$$f = 124.0 (1.2)_{\text{stat+fit}} (0.7)_{\text{syst}} [1.4] \text{ MeV} , \quad (58)$$

$$\bar{\ell}_4^{phys} = 3.43 (28)_{\text{stat+fit}} (36)_{\text{syst}} [46] , \quad (59)$$

which nicely agree with the corresponding results obtained by the analysis of f_π given by Eqs. (53-55). Note that the determination of w_0 obtained using X_π is more precise than the one from f_π by a factor equal to ≈ 2.5 .

Our result (57) is slightly larger than both the MILC result $w_0 = 0.1714^{+15}_{-12}$ fm from Ref. [15] and the HPQCD result $w_0 = 0.1715 (9)$ fm from Ref. [16], obtained using the

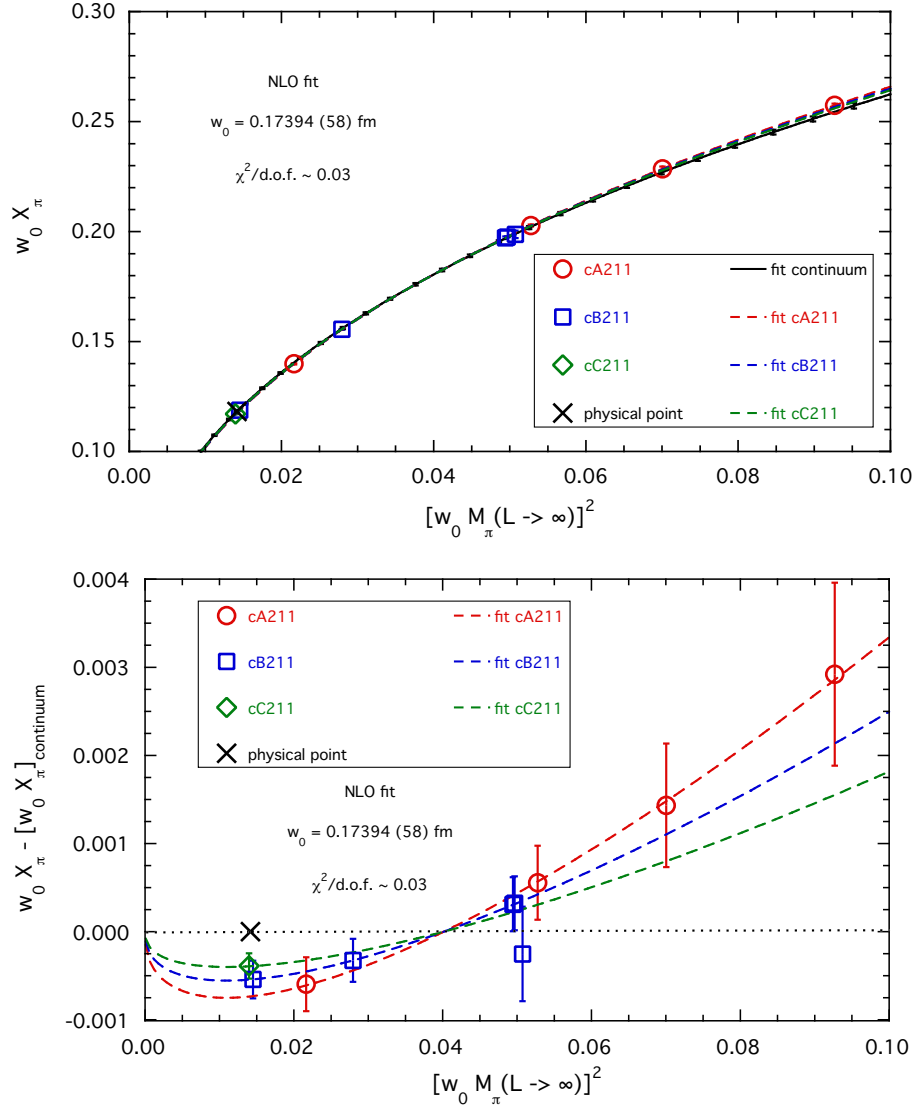


FIG. 6. *Top panel:* values of the quantity $w_0 X_\pi$ (open markers) compared to the results of the NLO fit corresponding to $A'_2 = F_{FVE} = 0$ in Eq. (56) applied to all data points ($M_\pi \lesssim 350$ MeV). The solid line represents the results of the fit in the continuum limit, while the dashed lines correspond to the fit evaluated at each value of β . The cross represents the result at the physical pion point (4) corresponding to the value $w_0 = 0.17394(58)$ fm. *Bottom panel:* the quantity $w_0 X_\pi$ after subtraction of its extrapolation to the continuum limit. The discretization terms proportional both to a^2 and to $a^2 \xi$ present in Eq. (56) are clearly visible.

value (6) to set the lattice scale. Within $\simeq 1.5$ standard deviations it is consistent with the recent, precise BMW determination $w_0 = 0.17236$ (70), obtained in Ref. [17] using the Ω^- -baryon mass to set the lattice scale. Furthermore, the difference with the recent result $w_0 = 0.1709(11)$ fm, obtained in Ref. [18] using the Ω^- -baryon mass to set the lattice scale, is within ~ 2 standard deviations.

In Appendix D 2 the procedure used in this Section to determine the GF scale w_0 is repeated in the case of the scales $\sqrt{t_0}$ and t_0/w_0 , obtaining

$$\sqrt{t_0} = 0.14436 \text{ (54)}_{\text{stat+fit}} \text{ (30)}_{\text{syst}} [61] \text{ fm} , \quad (60)$$

$$f = 124.1 \text{ (1.2)}_{\text{stat+fit}} \text{ (0.7)}_{\text{syst}} [1.4] \text{ MeV} , \quad (61)$$

$$\bar{\ell}_4^{\text{phys}} = 3.37 \text{ (27)}_{\text{stat+fit}} \text{ (38)}_{\text{syst}} [47] \quad (62)$$

and

$$t_0/w_0 = 0.11969 \text{ (52)}_{\text{stat+fit}} \text{ (33)}_{\text{syst}} [62] \text{ fm} , \quad (63)$$

$$f = 124.2 \text{ (1.4)}_{\text{stat+fit}} \text{ (0.8)}_{\text{syst}} [1.6] \text{ MeV} , \quad (64)$$

$$\bar{\rho}_4^{\text{phys}} = 3.31 \text{ (27)}_{\text{stat+fit}} \text{ (40)}_{\text{syst}} [48] . \quad (65)$$

Our finding (60) is larger than the MILC result $\sqrt{t_0} = 0.1416_{-5}^{+8}$ fm from Ref. [15] and the HPQCD result $\sqrt{t_0} = 0.1420$ (8) fm from Ref. [16], while within $\simeq 1.5$ standard deviations it is consistent with the recent result $\sqrt{t_0} = 0.1422(14)$ fm from Ref. [18].

The values of the lattice spacing corresponding to the three GF scales are collected in Table XII of Appendix D 2.

V. SU(2) CHPT ANALYSIS OF f_K/f_π

The kaon correlator

$$C_K(t) = \frac{1}{L^3} \sum_{x,z} \langle 0 | \bar{q}_s(x) \gamma_5 q_\ell(x) \bar{q}_\ell(z) \gamma_5 q_s(z) | 0 \rangle \delta_{t,(t_x-t_z)} \quad (66)$$

has been evaluated for three values of the (valence) strange bare quark mass $a\mu_s$ at each value of β , namely: $a\mu_s = \{0.0176, 0.0200, 0.0264\}$ for the ensembles cA211, $a\mu_s =$

$\{0.0148, 0.0185, 0.0222\}$ for the ensembles cB211 and $a\mu_s = \{0.0128, 0.0161, 0.0193\}$ for the ensemble cC211.06.80.

At large time distances one has

$$C_K(t) \xrightarrow[t \gg a, (T-t) \gg a]{} \frac{\mathcal{Z}_K}{2M_K} \left[e^{-M_K t} + e^{-M_K(T-t)} \right], \quad (67)$$

which allows the extraction of the kaon mass M_K and the matrix element $\mathcal{Z}_K = |\langle K | \bar{q}_s \gamma_5 q_\ell | 0 \rangle|^2$ from the exponential fit given in the r.h.s. of Eq. (67). The kaon decay constant f_K is given by

$$af_K = (a\mu_\ell + a\mu_s) \frac{\sqrt{a^4 \mathcal{Z}_K}}{aM_K \sinh(aM_K)} \quad (68)$$

and, using the pion data (16) for f_π , the ratio f_K/f_π is evaluated at each simulated strange bare quark mass. The time intervals $[t_{min}, t_{max}]$ adopted for the fit (67) of the kaon correlation function (66) are the same as those used for the case of the pion correlator, collected in Table II.

As in the case of the pion data (see Section II), due to a small deviation from maximal twist, a correction should be applied to observables of the ensemble cA211.12.48. We use the following formula (see Appendix B)

$$f_K|_{corrected} \simeq f_K \cdot K_f \quad (69)$$

with

$$K_f = \frac{1}{\cos[(\theta_s + \theta_\ell)/2]}, \quad (70)$$

where, we remind,

$$\frac{1}{\cos(\theta_i)} \equiv K_i = \sqrt{1 + (Z_A m_{PCAC}/\mu_i)^2}, \quad (71)$$

m_{PCAC} is the bare untwisted PCAC mass, Z_A is the renormalization constant of the axial current and μ_i is the bare twisted mass of the valence quarks. In the degenerate case $m_s = m_\ell$ one gets $K_f = K_\ell$, i.e. Eq. (19), while for $m_s \gg m_\ell$ one has $K_f \simeq 1/\cos(\theta_\ell/2)$.

Since the LECs of the SU(2) ChPT depend on the value of the (renormalized) strange quark mass m_s , we need to interpolate the ratio f_K/f_π at an approximately fixed value

of m_s . To this end we take advantage of the fact that the meson mass combination $2M_K^2 - M_\pi^2$ is proportional to m_s at LO in ChPT. Thus, for each gauge ensemble, adopting a simple quadratic spline, the lattice data for f_K/f_π are interpolated at a reference kaon mass given by

$$M_K^{ref} \equiv \sqrt{\left(M_K^{isoQCD}\right)^2 + \frac{M_\pi^2 - \left(M_\pi^{isoQCD}\right)^2}{2}} \quad (72)$$

with M_π^{isoQCD} and M_K^{isoQCD} chosen as in Eqs. (4) and (5), respectively. The physical units for M_π (and consequently for M_K^{ref}) are obtained by using the results for the lattice spacing given in Table XII of Appendix D 2 for each choice of the GF scale. In what follows we make use of our determination (57) of the GF scale w_0 . In this way the renormalized strange quark mass m_s^{ref} corresponding to M_K^{ref} is kept close to its physical value.

The results obtained for the ratio f_K/f_π interpolated at the kaon reference mass (72) are shown in Fig. 7 for all the ETMC gauge ensembles. The statistical errors of the data lie in the range $0.1 \div 0.6\%$.

We now apply the correction for FVEs using the GL formula and the expansion variable $\bar{\xi}_\pi$ defined as

$$\bar{\xi}_\pi \equiv \frac{M_\pi^2(L)}{(4\pi f)^2}, \quad (73)$$

where f is fixed at the value given by Eq. (58). For the pion and kaon decay constants the NLO FVE corrections are respectively given by [24]

$$\Delta_{FVE}^\pi(L) = -2\bar{\xi}_\pi \tilde{g}_1(M_\pi L) \quad (74)$$

$$\Delta_{FVE}^K(L) = -\frac{3}{4}\bar{\xi}_\pi \tilde{g}_1(M_\pi L), \quad (75)$$

so that the overall FVE correction for f_K/f_π is given by

$$\frac{f_K}{f_\pi}(L \rightarrow \infty) = \frac{f_K}{f_\pi}(L) \left[1 - \frac{5}{4}\bar{\xi}_\pi \tilde{g}_1(M_\pi L) \right]. \quad (76)$$

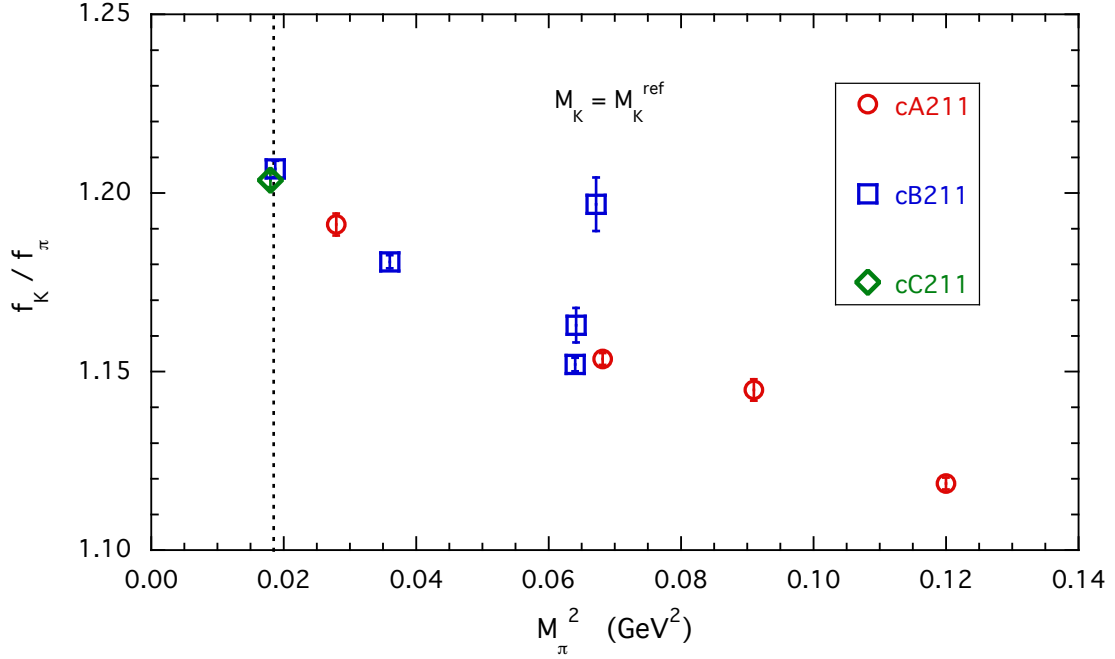


FIG. 7. Values of the ratio f_K/f_π interpolated at the kaon reference mass (72) versus the squared pion mass. The vertical dotted line indicates the location of the physical isoQCD point (4). For the ensemble cA211.12.48 the corrected value of the ratio f_K/f_π , obtained using Eqs. (18) and (69), is considered.

Finally, in terms of the variable ξ , defined in Eq. (46), the data for $(f_K/f_\pi)(L \rightarrow \infty)$ are fitted using the following ansatz

$$\frac{f_K}{f_\pi}(L \rightarrow \infty) = R_0 \left[1 + \frac{5}{4} \xi \log(\xi) + R_1 \xi + R_2 \xi^2 + \frac{a^2}{w_0^2} (\tilde{D}_0 + \tilde{D}_1 \xi) \right] \quad (77)$$

where with respect to the well-known SU(2) ChPT prediction at NLO a quadratic term in ξ as well as discretization effects proportional to a^2 and $a^2 M_\pi^2$ have been added.

The free parameters appearing in Eq. (77) are R_0 , R_1 , R_2 , \tilde{D}_0 , \tilde{D}_1 and their values are obtained by a straightforward χ^2 -minimization procedure. We have performed several fits based on Eq. (77) and the results for the ratio $(f_K/f_\pi)^{isoQCD}$ at the physical pion point (4) are collected in Table IV.

The quality of the NLO fit with $R_2 = \tilde{D}_1 = 0$ is illustrated in Fig. 8. It can be seen that FVEs are properly taken care of and that discretization effects are quite small.

$R_2 \neq 0$	$\tilde{D}_1 \neq 0$	range of M_π	$(f_K/f_\pi)^{isoQCD}$	$\chi^2/(d.o.f.)$
no	no	< 350 MeV	1.1995 (35)	0.53
no	yes	< 350 MeV	1.1984 (54)	0.58
no	no	< 190 MeV	1.2005 (48)	1.40
yes	no	< 350 MeV	1.1998 (32)	0.37

TABLE IV. Results for the decay constant ratio $(f_K/f_\pi)^{isoQCD}$ at the physical isoQCD point, given by Eqs. (4) and (5), obtained using the fitting function (77).

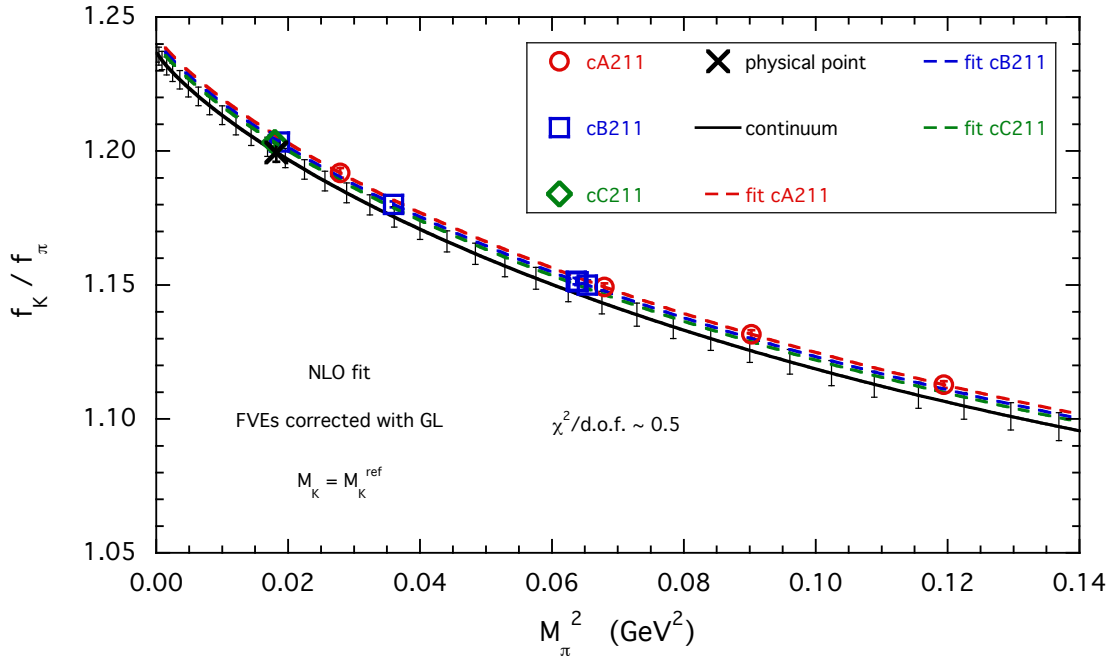


FIG. 8. Values of the ratio f_K/f_π corrected for FVEs according to Eq. (76) (open markers) compared to the results of the NLO fit corresponding to $R_2 = \tilde{D}_1 = 0$ in Eq. (77) applied to all pion masses ($M_\pi \lesssim 350$ MeV). The solid line represents the results of the fit in the continuum limit, while the dashed lines correspond to the fit evaluated at each value of β . The cross represents the result at the physical pion point (4).

As a check of the impact of FVEs we multiply the GL correction in Eq. (76) by a factor κ_{FVE} , which is treated as a further free parameter in the NLO fit. The factor κ_{FVE} turns out to be consistent with unity, $\kappa_{FVE} = 1.19(24)$, and the NLO result

$(f_K/f_\pi)^{isoQCD} = 1.1995$ (35) is reassuringly confirmed.

Putting together all the various results we obtain

$$\left(\frac{f_K}{f_\pi}\right)^{isoCQD} = 1.1995 \text{ (44)}_{stat+fit} \text{ (7)}_{syst} [44] , \quad (78)$$

where we remind that $(\)_{stat+fit}$ incorporates the uncertainties induced by both the statistical errors and the fitting procedure itself. Adopting the results of the ODE procedure (see Appendix B) for the extraction of the pion and kaon masses and decay constants the analysis of the ratio f_K/f_π yields

$$\left(\frac{f_K}{f_\pi}\right)^{isoCQD} = 1.1994 \text{ (43)}_{stat+fit} \text{ (7)}_{syst} [43] , \quad (79)$$

which compares very well with the finding (78).

The present result (78) improves drastically the precision of the previous $N_f = 2+1+1$ ETMC determination $(f_K/f_\pi)^{isoQCD} = 1.188$ (15) [20] by a factor of $\simeq 3.5$ reaching the level of $\simeq 0.4\%$. For comparison, the $N_f = 2 + 1 + 1$ determinations, entering the FLAG-4 average [19] and corrected for strong IB effects, yield a consistent value within the uncertainties, namely $(f_K/f_\pi)^{isoQCD} = 1.1966$ (18) [16, 20, 21]. Our finding (78) is also in good agreement with the recent determination $(f_K/f_\pi)^{isoQCD} = 1.1964$ (44) obtained in Ref. [36] adopting the same isoQCD prescription in a mixed-action approach (domain-wall valence quarks with staggered sea quarks).

VI. IMPLICATIONS FOR V_{us} AND THE FIRST-ROW CKM UNITARITY

Inserting our isoQCD result (78) into Eq. (3) the ratio of the CKM entries V_{us} and V_{ud} is given by

$$\left|\frac{V_{us}}{V_{ud}}\right| = 0.23079 \text{ (24)}_{exp} \text{ (87)}_{th} = 0.23079 \text{ (90)} . \quad (80)$$

Using the value $|V_{ud}| = 0.97370$ (14) from super-allowed nuclear beta decays [3, 22], which updates the old result $V_{ud} = 0.97420$ (21) from Ref. [9], Eq. (3) yields the following value for the CKM element $|V_{us}|$:

$$|V_{us}| = 0.22472 \text{ (24)}_{exp} \text{ (84)}_{th} = 0.22472 \text{ (87)} , \quad (81)$$

which is in good agreement with the latest estimate $|V_{us}| = 0.2252$ (5) from leptonic modes provided by the PDG [3].

Using the values $|V_{ub}| = 0.00382$ (24) [3] and $|V_{ud}| = 0.97370$ (14) [3, 22] our result (81) implies for the unitarity of the first-row of the CKM matrix the value

$$|V_{ud}|^2 + |V_{us}|^2 + |V_{ub}|^2 = 0.99861 \quad (48) , \quad (82)$$

which in turn would imply a $\simeq 3\sigma$ tension with unitarity from leptonic modes. Had we used the result $V_{ud} = 0.97420$ (21) from Ref. [9] the first-row CKM unitarity would be fulfilled within one standard deviation, i.e. within a precision of $\simeq 0.5$ permil.

Another source of information on V_{us} is represented by the semileptonic $K_{\ell 3}$ decay. In this case the relevant hadronic quantity is the vector form factor at zero momentum transfer $f_+(0)$. From the high-precision experimental data on $K_{\ell 3}$ decays one has $V_{us}f_+(0) = 0.2165$ (4) [37].

Using the ETMC determination $f_+(0) = 0.9709$ (46) obtained with Wilson twisted-mass quarks in Ref. [38], one gets the semileptonic result $V_{us} = 0.2230$ (11) to be compared with the leptonic one given in Eq. (81). The above finding is combined with Eq. (80) to obtain the red ellipse in Fig. 9, which represents a 68% likelihood contour. For comparison the blue ellipse corresponds to the FLAG-4 contour for $N_f = 2 + 1 + 1$ [19], defined by the bands corresponding to $V_{us} = 0.2231$ (7) and $V_{us}/V_{ud} = 0.2313$ (5). The two determinations of V_{ud} obtained in Refs. [9] and [22] are also shown. Finally, the dotted line represents the correlation between V_{us} and V_{ud} when the CKM matrix is taken to be unitary.

VII. CONCLUSIONS

We have presented a determination of the ratio of kaon and pion leptonic decay constants in isoQCD, f_K/f_π , adopting the gauge ensembles produced by ETMC with $N_f = 2 + 1 + 1$ flavors of Wilson-clover twisted-mass quarks, including configurations close to the physical point for all dynamical flavors.

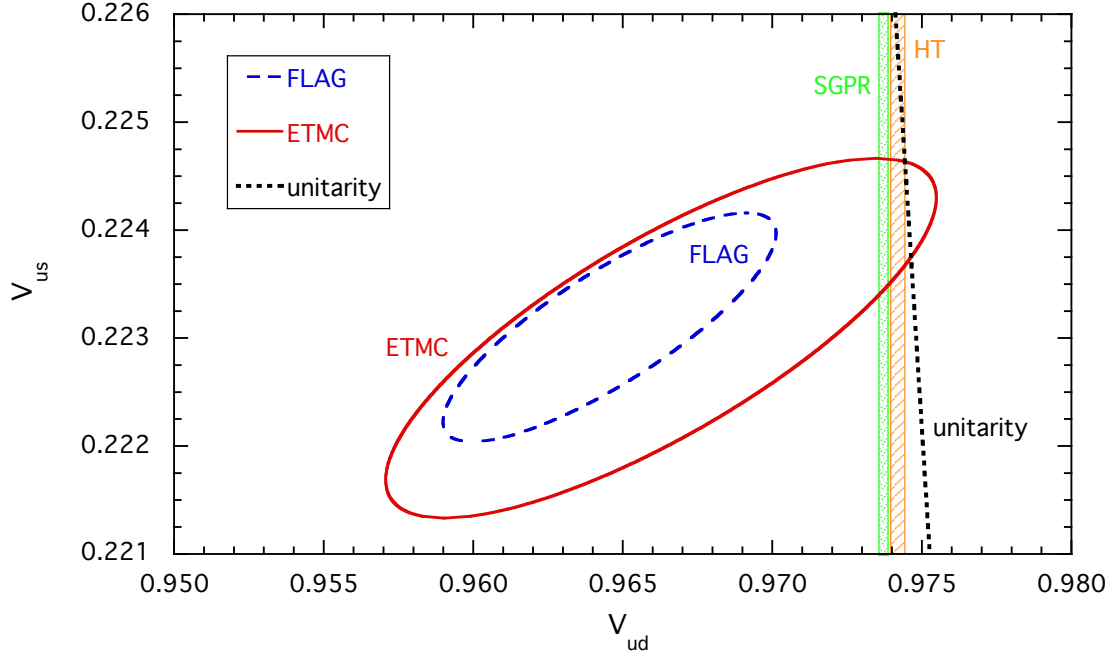


FIG. 9. The plot compares the information for V_{ud} and V_{us} obtained in the FLAG-4 review for $N_f = 2 + 1 + 1$ [19] and in this work by using Eq. (80) and the semileptonic result of Ref. [38]. The determinations of V_{ud} obtained from superallowed nuclear β transitions obtained in Refs. [9, 22] are also shown as green and orange bands, labelled respectively HT and SGPR. The dotted line indicates the correlation between V_{ud} and V_{us} that follows assuming the unitarity of the CKM-matrix. The ellipses represent 68% likelihood contours.

The simulations are carried out at three values of the lattice spacing ranging from ~ 0.068 to ~ 0.092 fm with linear lattice size up to $L \sim 5.5$ fm. The scale is set using the value the pion decay constant $f_\pi^{isoQCD} = 130.4(2)$ MeV taken from Ref. [8]. Two observables, f_π and $(f_\pi M_\pi^4)^{1/5}$, have been analyzed within the framework of SU(2) ChPT without making use of renormalized quark masses. The latter quantity is found to be marginally affected by lattice artifacts and provides a precise determination of the GF scales, namely: $w_0 = 0.17383(63)$ fm, $\sqrt{t_0} = 0.14436(61)$ fm and $t_0/w_0 = 0.11969(62)$ fm.

As for the decay constant ratio f_K/f_π we get at the physical isoQCD point, defined

by Eqs. (4-6), the result

$$\left(\frac{f_K}{f_\pi}\right)^{isoQCD} = 1.1995 \quad (44) , \quad (83)$$

where the error includes both statistical and systematic uncertainties in quadrature. Our result (83) agrees nicely with the recent $N_f = 2 + 1 + 1$ determinations, entering the FLAG-4 average [19] and corrected for strong IB effects, namely $(f_K/f_\pi)^{isoQCD} = 1.1966$ (18) [16, 20, 21].

Taking the updated value $|V_{ud}| = 0.97370$ (14) from super-allowed nuclear beta decays [3, 22], Eqs. (3) and (83) yield the following value for the CKM element $|V_{us}|$:

$$|V_{us}| = 0.22472 \quad (24)_{\text{exp}} \quad (84)_{\text{th}} = 0.22472 \quad (87) , \quad (84)$$

which is nicely consistent with the latest estimate $|V_{us}| = 0.2252$ (5) from leptonic modes provided by the PDG [3]. Correspondingly, using $|V_{ub}| = 0.00382$ (24) [3] the first-row CKM unitarity becomes

$$|V_{ud}|^2 + |V_{us}|^2 + |V_{ub}|^2 = 0.99861 \quad (48) , \quad (85)$$

which would imply a $\simeq 3\sigma$ tension with unitarity from leptonic modes.

ACKNOWLEDGMENTS

We thank all the ETMC members for a very productive collaboration. We warmly thank G.C. Rossi for his continuous support and for a careful reading of the manuscript. We are grateful to B. Joó for his kind support with our refactoring and extension of the QPhiX lattice QCD library.

We acknowledge PRACE (Partnership for Advanced Computing in Europe) for awarding us access to the high-performance computing system Marconi and Marconi100 at CINECA (Consorzio Interuniversitario per il Calcolo Automatico dell'Italia Nord-orientale) under the grants Pra17-4394, Pra20-5171 and Pra22-5171, and CINECA for providing us CPU time under the specific initiative INFN-LQCD123. We also acknowledge PRACE for awarding us access to HAWK, hosted by HLRS, Germany, under the

grant with Acid 33037. The authors gratefully acknowledge the Gauss Centre for Supercomputing e.V. (www.gauss-centre.eu) for funding the project pr74yo by providing computing time on the GCS Supercomputer SuperMUC at Leibniz Supercomputing Centre (www.lrz.de). Some of the ensembles for this study were generated on Jureca Booster [39] and Juwels [40] at the Jülich Supercomputing Centre (JSC) and we gratefully acknowledge the computing time granted there by the John von Neumann Institute for Computing (NIC).

The project has received funding from the Horizon 2020 research and innovation program of the European Commission under the Marie Skłodowska-Curie grant agreement No 642069 (HPC-LEAP) and under grant agreement No 765048 (STIMULATE). The project was funded in part by the NSFC (National Natural Science Foundation of China) and the DFG (Deutsche Forschungsgemeinschaft, German Research Foundation) through the Sino-German Collaborative Research Center grant TRR110 “Symmetries and the Emergence of Structure in QCD” (NSFC Grant No. 12070131001, DFG Project-ID 196253076 - TRR 110).

R.F. acknowledges the University of Rome Tor Vergata for the support granted to the project PLNUGAMMA. F.S. and S.S. are supported by the Italian Ministry of Research (MIUR) under grant PRIN 20172LNEEZ. F.S. is supported by INFN under GRANT73/CALAT. P.D. acknowledges support from the European Unions Horizon 2020 research and innovation programme under the Marie Skłodowska-Curie grant agreement No. 813942 (EuroPLEx) and from INFN. under the research project INFN-QCDLAT. S.B. and J.F. are supported by the H2020 project PRACE6-IP (grant agreement No 82376) and the COMPLEMENTARY/0916/0015 project funded by the Cyprus Research Promotion Foundation. The authors acknowledge support from project NextQCD, co-funded by the European Regional Development Fund and the Republic of Cyprus through the Research and Innovation Foundation (EXCELLENCE/0918/0129).

Appendix A: Algorithmic details and parameters for the ETMC gauge ensembles

In Appendix A 1, we present the algorithmic setup employed for the generation of our ensembles of gauge configurations, while the simulation parameters are given in Table V.

ensemble	β	c_{SW}	κ	V/a^4	$a\mu_\ell$	$a\mu_\sigma$	$a\mu_\delta$	λ_{min}	λ_{max}
cA211.53.24	1.726	1.74	0.1400645	$24^3 \times 48$	0.00530	0.1408	0.1521	0.0000376	4.7
cA211.40.24				$24^3 \times 48$	0.00400				
cA211.30.32				$32^3 \times 64$	0.00300				
cA211.12.48			0.1400650	$48^3 \times 96$	0.00120				
cB211.25.24	1.778	1.69	0.1394267	$24^3 \times 48$	0.00250	0.1246864	0.131052	0.0000344	4.3
cB211.25.32				$32^3 \times 64$	0.00250				
cB211.25.48				$48^3 \times 96$	0.00250				
cB211.14.64				$64^3 \times 128$	0.00140				
cB211.072.64			0.1394265	$64^3 \times 128$	0.00072				
cC211.06.80	1.836	1.6452	0.13875285	$80^3 \times 160$	0.00060	0.106586	0.107146	0.0000376	4.7

TABLE V. Simulation parameters for the ensembles used for this study. Please refer to Appendix A 1 for details on the integrator setup.

1. Integrator Setups

In the generation of gauge ensembles via the Hybrid Monte Carlo algorithm, the effective lattice action can be represented by a sum over *monomials* corresponding to different contributions to the partition function as defined below. In the integration of the equations of motion, the forces contributed by the different monomials differ by orders of magnitude, allowing them to be integrated on different time scales accordingly, as detailed in Table VI below.

a. Monomial Types

We define below the different types of monomials that we employ in our effective lattice action to simulate QCD using $N_f = 2 + 1 + 1$ twisted mass clover fermions.

Gauge: [gau(β, c_1)]

$$\frac{\beta}{3} \sum_x \left(c_0 \sum_{\substack{\mu, \nu=1 \\ 1 \leq \mu < \nu}}^4 \{1 - \text{Re Tr}(U_{x, \mu, \nu}^{1 \times 1})\} + c_1 \sum_{\substack{\mu, \nu=1 \\ \mu \neq \nu}}^4 \{1 - \text{Re Tr}(U_{x, \mu, \nu}^{1 \times 2})\} \right), \quad (\text{A1})$$

with $c_0 = (1 - 8c_1)$, for the Iwasaki action used here [25], $c_1 = -0.331$.

Degenerate Determinant: [det(ρ)]

The action contribution of a degenerate doublet of clover-improved twisted mass quarks is given by

$$\begin{aligned} S[\chi, \bar{\chi}, U] &= \sum_x \left\{ \bar{\chi}(x) [1 + 2\kappa c_{SW} T + 2i\kappa\mu\gamma_5\tau^3] \chi(x) \right. \\ &\quad - \kappa \bar{\chi}(x) \sum_{\mu=1}^4 \left[U_\mu(x) (r - \gamma_\mu) \chi(x + a\hat{\mu}) \right. \\ &\quad \left. \left. + U_\mu^\dagger(x - a\hat{\mu}) (r + \gamma_\mu) \chi(x - a\hat{\mu}) \right] \right\} \\ &\equiv \sum_{x, y} \bar{\chi}(x) M_{xy} \chi(y), \end{aligned} \quad (\text{A2})$$

in the twisted basis and in the hopping parameter normalisation, where T is the clover term. In our simulations we use the conventional value $r = 1$.

For convenience, we define $\tilde{\mu} \equiv 2\kappa\mu$ and absorb $2\kappa c_{SW}$ into T , defining the two-flavour operator

$$Q \equiv \gamma_5 M = \begin{pmatrix} Q_+ & \\ & Q_- \end{pmatrix}, \quad (\text{A3})$$

and the Hermitian operator $Q_{\text{sw}} = \gamma_5 D_{\text{sw}}$, where in turn D_{sw} is the clover-improved Wilson Dirac operator. We then have $Q_\pm = Q_{\text{sw}} \pm i\tilde{\mu}$, such that $Q_+^\dagger = Q_-$ and $Q_+ Q_- = Q_{\text{sw}}^2 + \tilde{\mu}^2$. The contribution to the partition function of the mass-degenerate (light) twisted mass quark doublet is thus given by $\det(Q_+ Q_-) = \det(Q_{\text{sw}}^2 + \tilde{\mu}^2)$.

An even-odd Schur decomposition of the sub-matrices Q_{\pm} then gives

$$\begin{aligned} Q^{\pm} &= \gamma_5 \begin{pmatrix} 1 + T_{ee} \pm i\tilde{\mu}\gamma_5 & M_{eo} \\ M_{oe} & 1 + T_{oo} \pm i\tilde{\mu}\gamma_5 \end{pmatrix} = \gamma_5 \begin{pmatrix} M_{ee}^{\pm} & M_{eo} \\ M_{oe} & M_{oo}^{\pm} \end{pmatrix} \\ &= \begin{pmatrix} \gamma_5 M_{ee}^{\pm} & 0 \\ \gamma_5 M_{oe} & 1 \end{pmatrix} \begin{pmatrix} 1 & (M_{ee}^{\pm})^{-1} M_{eo} \\ 0 & \gamma_5 (M_{oo}^{\pm} - M_{oe} (M_{ee}^{\pm})^{-1} M_{eo}) \end{pmatrix}, \end{aligned} \quad (\text{A4})$$

from which we obtain \hat{Q}_{\pm} defined only on the odd sites of the lattice

$$\hat{Q}_{\pm} = \gamma_5 \left(M_{oo}^{\pm} - M_{oe} (M_{ee}^{\pm})^{-1} M_{eo} \right). \quad (\text{A5})$$

The light quark determinant can then be reexpressed as

$$\det(Q_+ Q_-) = \det(M_{ee}^+ M_{ee}^-) \cdot \det(\hat{Q}_+ \hat{Q}_-). \quad (\text{A6})$$

In order to implement mass preconditioning, the \hat{Q}_{\pm} can be shifted by a constant through the addition of a further twisted mass: $\hat{W}_{\pm}(\rho) = \hat{Q}_{\pm} \pm i\rho$, such that $\hat{W}_+ \hat{W}_- = \hat{Q}_+ \hat{Q}_- + \rho^2$. It should be noted that this shift is applied to the even-odd-preconditioned operator, such that the factor M_{ee}^{\pm} remains independent of ρ since its inverse is non-trivial.

In terms of pseudofermion fields, one thus obtains a contribution to the partition function

$$\int \mathcal{D}\phi_1^{\dagger} \mathcal{D}\phi_1 \exp \left\{ -\phi_1^{\dagger} (\hat{W}_+ \hat{W}_-)^{-1} \phi_1 \right\}, \quad (\text{A7})$$

which we refer to as the degenerate determinant and a corresponding contribution

$$\int \mathcal{D}\phi_2^{\dagger} \mathcal{D}\phi_2 \exp \left\{ -\phi_2^{\dagger} \hat{W}_- \frac{1}{\hat{Q}_+ \hat{Q}_-} \hat{W}_+ \phi_2 \right\}, \quad (\text{A8})$$

which we refer to as a determinant ratio.

Determinant Ratio: $[\text{detrat}(\rho_b, \rho_t)]$

Eq. (A8) generalises to the introduction of multiple shifts $\rho_1, \rho_2, \dots, \rho_n$ to contributions of the form:

$$\int \mathcal{D}\phi_i^{\dagger} \mathcal{D}\phi_i \exp \left\{ -\phi_i^{\dagger} \hat{W}_- (\rho_t) \frac{1}{\hat{W}_+ (\rho_b) \hat{W}_- (\rho_b)} \hat{W}_+ (\rho_t) \phi_i \right\}. \quad (\text{A9})$$

The pseudofermion fields ϕ_i are defined only on the odd sites of the lattice and are generated from a random spinor field R_i , sampled from a normalized Gaussian distribution at the beginning of each molecular dynamics trajectory. In the case of the determinant, we have $\phi_i = \hat{Q}_+ R_i$, while in the case of the determinant ratio we have $\phi_j = \left(\hat{W}_+(\rho_t)\right)^{-1} \hat{W}_+(\rho_b) R_j$.

The complete mass-preconditioned contribution with n shifts is thus given by

$$\det(\rho_n) \cdot \text{detrat}(\rho_{n-1}, \rho_n) \cdot \text{detrat}(\rho_{n-2}, \rho_{n-1}) \cdot \dots \cdot \text{detrat}(0, \rho_1), \quad (\text{A10})$$

where the last factor has the form of Eq. (A8) with the target twisted quark mass in \hat{Q}_\pm . In general, the different contributions are integrated on multiple time scales because their contributions to the force differ by orders of magnitude.

Rational Approximation Partial Fraction: [rat(n_ℓ, n_k)]

The Dirac operator for the non-degenerate flavour doublet employed in the strange-charm sector reads

$$D_h(\bar{\mu}, \bar{c}) = D_{\text{sw}} \cdot 1_f + i\bar{\mu}\gamma_5\tau_f^3 - \bar{c}\tau_f^1, \quad (\text{A11})$$

with the property

$$D_h^\dagger = \tau_f^1\gamma_5 D_h \gamma_5 \tau_f^1. \quad (\text{A12})$$

Equivalently, as used (without the clover term) in Ref. [41], one may write

$$D'_h(\mu_\sigma, \mu_\delta) = D_{\text{sw}} \cdot 1_f + i\mu_\sigma\gamma_5\tau_f^1 + \mu_\delta\tau_f^3, \quad (\text{A13})$$

which is related to D_h by $D'_h = (1 + i\tau_f^2)D_h(1 - i\tau_f^2)/2$ and $(\mu_\sigma, \mu_\delta) \rightarrow (\bar{\mu}, -\bar{c})$.

As before, we define $Q_h = \gamma_5 D_h$ and the implementation of even-odd preconditioning translates straightforwardly from the mass-degenerate case, although the construction of M_{ee}^h has to take into account the additional (off-diagonal) flavour structure.

The operator \hat{Q}_h , defined only on the odd sites, has the property $\hat{Q}_h^\dagger = \tau_f^1 \hat{Q}_h \tau_f^1$ and the non-degenerate quark doublet contributes a factor

$$\det(Q_h) \propto \det(\hat{Q}_h) \quad (\text{A14})$$

to the partition function, which we simulate via

$$\left[\det(\hat{Q}_h^2) \right]^{1/2} \approx \det(\mathcal{R}^{-1}) , \quad (\text{A15})$$

where we made use of the shorthand notation $\hat{Q}_h^2 = \hat{Q}_h \tau_f^1 \hat{Q}_h \tau_f^1$.

We use a rational approximation of order N (see Refs. [42–44])

$$\mathcal{R}(\hat{Q}_h^2) = A \prod_{i=1}^N \frac{\hat{Q}_h^2 + a_{2i}}{\hat{Q}_h^2 + a_{2i-1}} \approx \frac{1}{\sqrt{\hat{Q}_h^2}} . \quad (\text{A16})$$

For this, we employ the Zolotarev solution [45] for the optimal approximation to $1/\sqrt{y}$, where the coefficients a_i satisfy the property

$$a_1 > a_2 > \dots > a_{2N} > 0 . \quad (\text{A17})$$

The amplitude A , the coefficients a_i and the maximal deviation of the rational approximation $\delta = \max_y |1 - \sqrt{y} \mathcal{R}(y)|$ are computed analytically at given order N and lower bound $\epsilon < y < 1$. These are

$$a_i = \text{cs}^2(i \cdot v, \sqrt{1 - \epsilon}) \quad \text{with } v = \frac{K(\sqrt{1 - \epsilon})}{2N + 1} \quad (\text{A18})$$

$$A = \frac{2}{1 + \sqrt{1 - d^2}} \prod_{j=1}^N \frac{s_{2j-1}}{s_{2j}} \quad \text{with } s_i = \text{sn}^2(i \cdot v, \sqrt{1 - \epsilon}) \quad (\text{A19})$$

$$\delta = \frac{d^2}{1 + \sqrt{1 - d^2}} \quad \text{with } d = (1 - \epsilon)^{\frac{2N+1}{2}} \prod_{j=1}^N s_{(2j-1)}^2 \quad (\text{A20})$$

where $\text{sn}(u, k)$ and $\text{cs}(u, k) = \text{cn}(u, k)/\text{sn}(u, k)$ are Jacobi elliptic functions and $K(k)$ is the complete elliptic integral. In all our simulations we use $N = 10$ and $\epsilon = \lambda_{\min}/\lambda_{\max}$ where λ_{\min} and λ_{\max} are respectively the lower and upper bound of the eigenvalues of \hat{Q}_h^2 . In order to have all the eigenvalues λ in the range $\epsilon < \lambda < 1$, we re-scale \hat{Q}_h^2 with λ_{\max} . The values of λ_{\min} and λ_{\max} per ensemble are given in

Table V. In the simulation, we explicitly check that the eigenvalues of \hat{Q}_h^2 remain within these bounds.

The factors in the approximation can be grouped

$$\mathcal{R}(\hat{Q}_h^2) = Ar_1^\ell(\hat{Q}_h^2) \cdot r_\ell^k(\hat{Q}_h^2) \cdot \dots, \quad (\text{A21})$$

where

$$r_{n_\ell}^{n_k}(\hat{Q}_h^2) = \prod_{i=n_\ell}^{n_k} \frac{\hat{Q}_h^2 + a_{2i-1}}{\hat{Q}_h^2 + a_{2i}} = \text{rat}(n_\ell, n_k). \quad (\text{A22})$$

We perform partial fraction expansions of the terms

$$r_{n_\ell}^{n_k}(\hat{Q}_h^2) = 1 + \sum_{i=n_\ell}^{n_k} \frac{q_i}{\hat{Q}_h^2 + \mu_i^2}, \quad (\text{A23})$$

such that the necessary matrix inverse can be calculated efficiently using a multi-shift solver. The coefficients q_i are given by

$$q_i = (a_{2i-1} - a_{2i}) \prod_{m=n_\ell, m \neq i}^{n_k} \frac{a_{2m-1} - a_{2i}}{a_{2m} - a_{2i}}, \quad i = n_\ell, \dots, n_k. \quad (\text{A24})$$

We can further define $\mu_i = \sqrt{a_{2i}}$ and $\nu_i = \sqrt{a_{2i-1}}$ and express q_i as

$$q_i = (\nu_i^2 - \mu_i^2) \prod_{m=n_\ell, m \neq i}^{n_k} \frac{\nu_m^2 - \mu_i^2}{\mu_m^2 - \mu_i^2}, \quad i = n_\ell, \dots, n_k. \quad (\text{A25})$$

At the beginning of each trajectory, pseudofermion fields are generated as follows: again a random spinor field R is sampled from a Gaussian distribution. Now, we need to compute pseudofermion fields ϕ from

$$R^\dagger R = \phi^\dagger \mathcal{R} \phi$$

and, therefore, we need operators C^\dagger and C with the property

$$\mathcal{R}^{-1} = C^\dagger \cdot C, \quad \Rightarrow \quad \phi = C \cdot R.$$

C is given by (inspired by twisted mass)

$$C = \prod_{i=1}^N \frac{\hat{Q}_h + i\mu_i}{\hat{Q}_h + i\nu_i}$$

which can again be written as a partial fraction

$$C = 1 + i \sum_{i=1}^N \frac{r_i}{\hat{Q}_h + i\nu_i},$$

with

$$r_i = (\mu_i - \nu_i) \prod_{m=1, m \neq i}^N \frac{\mu_m - \nu_i}{\nu_m - \nu_i}, \quad i = 1, \dots, N.$$

The rational approximation \mathcal{R} can be applied to a vector using a multi-mass solver and the partial fraction representation. The same works for C : after solving N equations simultaneously for $(\hat{Q}_h^2 + \nu_i^2)^{-1}$, $i = 1, \dots, N$, we have to multiply every term with $(\hat{Q}_h - i\nu_i)$. The hermitian conjugate of C is given by

$$C^\dagger = 1 - i \sum_{i=1}^N \frac{r_i}{\hat{Q}_h - i\nu_i},$$

using $\hat{Q}_h^\dagger = \hat{Q}_h$. For the acceptance step only the application of \mathcal{R} is needed.

Rational Approximation Correction Factor: [ratcor(n)]

The rational approximation \mathcal{R} only has a finite precision. This finite precision can be accounted for during the acceptance step in the HMC by estimating [44] $1 - |\hat{Q}_h|\mathcal{R}$, if the rational approximation is precise enough. This can be achieved by including a monomial $\det(|\hat{Q}_h|\mathcal{R})$ in the simulation, for which one needs an operator B

$$B \cdot B^\dagger = |\hat{Q}_h|\mathcal{R}.$$

Following Ref. [44], B can be written as

$$B = (1 + Z)^{1/4} = \sum_{i=0}^m c_i Z^i = 1 + \frac{1}{4}Z - \frac{3}{32}Z^2 + \frac{7}{128}Z^3 + \dots$$

with $Z = \hat{Q}_h^2 \mathcal{R}^2 - 1$. The series converges rapidly and can, thus, be truncated after a few terms, $m + 1$. The convergence can actually be controlled during the simulation and the truncation does not need to be fixed. We choose to sum the series until the contribution of the given term to the acceptance Hamiltonian is

below the residual precision squared, r^2 , that we employ for the solution of the linear systems involved in the approximation of \mathcal{R} in the *acceptance step*, such that $|c_m Z_m \phi|^2 < r^2$, which we typically choose to be at the limit of double precision arithmetic.

For this monomial the pseudofermion field is computed from

$$\phi = B \cdot R,$$

where R is again a Gaussian random vector, see above.

b. Simulation parameters

In Table VI we list monomials and parameters used per ensemble. The monomials are grouped in various timescales where the one with the highest id is the outermost timescale (with the fewest integration steps) into which the other time scales are nested. For the various timescales two integrator types are used, either the second order minimal norm (2MN) integrator or its extension with a force gradient (2MNFG), making the latter a fourth-order integrator [46]. The number of steps per timescale is indicated with N_s .

The time evolution operator $\exp[(\delta\tau)H_{\text{MD}}]$ for a given MD-Hamiltonian can be decomposed into “kinetic” and “potential” parts, $\exp[(\delta\tau)(T + V)]$. To a given order n in the time step $\delta\tau$, this can be factorised

$$\exp[(\delta\tau)(T + V)] = \prod_{i=1}^n \exp[c_i(\delta\tau)T] \exp[d_i(\delta\tau)V] + \mathcal{O}[(\delta\tau)^{n+1}]. \quad (\text{A26})$$

By expanding the left-hand side of Eq. (A26) (being mindful of the non-commutativity of T and V) and matching the coefficients c_i and d_i of terms of equal order in $\delta\tau$, explicit factorizations can be constructed. In practice, the expansion of the left-hand side is only formal and one attempts instead to formulate order equations in the coefficients c_i and d_i to eliminate terms which are expensive to compute (stemming from commutators of T and V) to satisfy the equality to some approximation. For 2MN and 2MNFG, these equations can be reformulated in terms of a coefficient λ .

The 2MNFG scheme is now given by setting $\lambda = 1/6$, which cancels out one of the second order commutators $[T, [V, T]]$. Now, the remaining term $[V, [V, T]]$ can be canceled using the force gradient term. It turns out that for the 2MN integrator an optimal value for λ is larger than $1/6$. Namely assuming unity of the second order commutators and neglecting any correlations leads to the optimal value of $\lambda \approx 0.1931833275$. In the usage of the 2MN integrator with multiple time scales, experience suggests that further deviations from this optimal value improve the acceptance rate, such that we often use schemes with increasing values of λ from the innermost to the outermost time scale, as shown in Table VI.

2. Software details

The simulations presented in this study have been generated using the tmLQCD [47–49] software suite, which provides all the necessary components to perform $N_f = 2+1+1$ simulations of twisted mass clover fermions, including implementations of the polynomial and rational HMC algorithms for the non-degenerate determinant. To enable multigrid solvers to be used in simulations [50], tmLQCD provides an interface to DD α AMG [51], a multigrid solver library optimized for twisted mass (clover) fermions [52]. The force calculation of some monomials in the light quark sector is accelerated by a 3-level multi-grid approach. Moreover, we extended the DD α AMG method for the mass non-degenerate twisted mass operator. The multi-grid solver used in the rational approximation [53] is particularly helpful for the lowest terms of the rational approximation, as well as for the rational approximation corrections in the acceptance step, where it yields a speed up of two over the standard multi-mass shifted conjugate gradient (MMS-CG) solver on traditional distributed-memory machines based on Intel Skylake or AMD EPYC architectures.

On the other hand, especially on machines based on Intel’s Knight’s Landing (KNL) architecture, only the most poorly-conditioned monomials benefit from the usage of DD α AMG, to the point where (on KNL) the inversion of the non-degenerate operator

Id	Type	N_s	λ	Monomials	Id	Type	N_s	λ	Monomials
cA211.53.24, 5 timescales, $\tau = 1.0$					cB211.25.24/32, 4 timescales, $\tau = 1.5$				
0	2MN	1	0.193	gau(β, c_1)	0	2MNFG	1	0.167	gau(β, c_1)
1	2MN	1	0.195	det(0.1)	1	2MNFG	1	0.167	det(0.3), rat(0, 3)
2	2MN	1	0.197	detrat(0.02, 0.1), rat(0, 5)	2	2MNFG	1	0.167	detrat(0.045, 0.3), detrat(0.0045, 0.045), rat(4, 5)
3	2MN	1	0.200	detrat(0.003, 0.02), rat(6, 7)	3	2MN	13	0.193	detrat(0, 0.045), rat(6, 9)
4	2MN	9	0.205	detrat(0, 0.003), rat(8, 9)	cB211.25.48, 5 timescales, $\tau = 1.0$				
cA211.40.24, 5 timescales, $\tau = 1.0$					0	2MN	1	0.193	gau(β, c_1)
0	2MN	1	0.193	gau(β, c_1)	1	2MN	1	0.195	det(0.24)
1	2MN	1	0.195	det(0.1)	2	2MN	1	0.197	detrat(0.033, 0.24), rat(0, 5)
2	2MN	1	0.197	detrat(0.02, 0.1), rat(0, 5)	3	2MN	1	0.200	detrat(0.004, 0.033), rat(6, 7)
3	2MN	1	0.200	detrat(0.003, 0.02), rat(6, 7)	4	2MN	15	0.205	detrat(0, 0.004), rat(8, 9)
4	2MN	9	0.205	detrat(0, 0.003), rat(8, 9)	cB211.14.64, 4 timescales, $\tau = 1.5$				
cA211.30.32, 5 timescales, $\tau = 1.0$					0	2MNFG	1	0.167	gau(β, c_1)
0	2MN	1	0.193	gau(β, c_1)	1	2MNFG	1	0.167	det(0.2), rat(0, 3)
1	2MN	1	0.195	det(0.1)	2	2MNFG	1	0.167	detrat(0.02, 0.2), detrat(0.002, 0.02), rat(4, 5)
2	2MN	1	0.197	detrat(0.02, 0.1), rat(0, 5)	3	2MN	23	0.193	detrat(0, 0.002), rat(6, 9)
3	2MN	1	0.200	detrat(0.003, 0.02), rat(6, 7)	cB211.072.64, 6 timescales, $\tau = 1.0$				
4	2MN	12	0.205	detrat(0, 0.003), rat(8, 9)	0	2MN	1	0.185	gau(β, c_1)
cA211.12.48, 6 timescales, $\tau = 1.0$					1	2MN	1	0.190	det(0.1)
0	2MN	1	0.185	gau(β, c_1)	2	2MN	1	0.195	detrat(0.01, 0.1), rat(0, 2)
1	2MN	1	0.190	det(0.16)	3	2MN	1	0.200	detrat(0.0012, 0.01), rat(3, 5)
2	2MN	1	0.195	detrat(0.03, 0.16), rat(0, 2)	4	2MN	1	0.205	detrat(0.0003, 0.0012), rat(6, 7)
3	2MN	1	0.200	detrat(0.006, 0.03), rat(3, 4)	5	2MN	12	0.205	detrat(0, 0.0003), rat(8, 9)
4	2MN	1	0.205	detrat(0.001, 0.006), rat(5, 6)	cC211.06.80, 4 timescales, $\tau = 1.0$				
5	2MN	17	0.210	detrat(0, 0.001), rat(7, 9)	0	2MNFG	1	0.167	gau(β, c_1)
					1	2MNFG	1	0.167	det(0.12), rat(0, 3)
					2	2MNFG	1	0.167	detrat(0.012, 0.12), detrat(0.0012, 0.012), rat(4, 6)
					3	2MN	14	0.193	detrat(0, 0.0012), rat(7, 9)

TABLE VI. Integrators setup used for the ensembles analyzed in this study. The number of time scales and trajectory length, τ , used for each ensemble are indicated in the respective headers.

does not benefit at all. To improve efficiency, tmLQCD also provides an interface to the QPhiX [54] lattice QCD library, which we have refactored and extended [55] to support twisted mass clover fermions, including the non-degenerate doublet. For solves related to the degenerate determinant and determinant ratios, this allows us to efficiently and flexibly combine mixed-precision CG and SIMD vector lengths of 8 or 16 as required by AVX512. On KNL, single-precision QPhiX kernels are up to a factor of 5 more

efficient than their tmLQCD-native equivalents. Also in the MMS-CG solves in the non-degenerate sector, the double-precision kernels in QPhiX are up to a factor of 2 more efficient than the tmLQCD-native equivalents on KNL. Combined, these efficiency improvements lead to overall speedup factors of 2-3 in the HMC on this architecture with smaller overall gains on Skylake and EPYC.

Appendix B: Extraction of aM_π and af_π using the ODE procedure

The spectral decomposition of the pion correlation function (14) can be investigated adopting the ODE procedure of Ref. [23]. This method is able to extract exponential signals from the temporal dependence of a lattice correlator without any *a priori* knowledge of the multiplicity of each signal and it does not require any starting input for the masses and the amplitudes of the signals.

The ODE approach is sensitive to the noise of the correlator, so that pure oscillating signals (conjugate pairs of imaginary masses) may typically appear in the ODE spectral decomposition. Therefore, we adopt an improved version of the ODE procedure, in which a subsequent χ^2 -minimization procedure is applied to the non-noisy part of the ODE spectral decomposition [23]. In this way the accuracy of the *physical* (i.e. non-noisy) part of the ODE spectral decomposition is improved.

The time intervals $[t_{min}, t_{max}]$ adopted for the analysis and the extracted values of the pion mass and decay constant in lattice units are collected in Table VII.

Within the ODE procedure we searched for 8 exponential signals in the time intervals of Table VII and in all cases at least two physical (non-noisy) exponential signals were found. Then, a χ^2 -minimization procedure was applied using the physical ODE solution as the starting point. The minimized values of the χ^2 variable turned out to be always less than 1.

The extracted values as well as their statistical errors of the ground-state mass and decay constant, collected in Table VII, are nicely consistent with the corresponding ones obtained by the direct single exponential fit (15) shown in Table II.

ensemble	β	V/a^4	$[t_{\min}/a, t_{\max}/a]$	aM_π	af_π
cA211.53.24	1.726	$24^3 \times 48$	[5, 24]	0.16621 (40)	0.07106 (36)
cA211.40.24		$24^3 \times 48$	[5, 24]	0.14473 (76)	0.06809 (30)
cA211.30.32		$32^3 \times 64$	[6, 32]	0.12523 (18)	0.06675 (15)
cA211.12.48		$48^3 \times 96$	[6, 48]	0.08000 (28)	0.06139 (34)
cB211.25.24	1.778	$24^3 \times 48$	[6, 24]	0.10750 (189)	0.05351 (48)
cB211.25.32		$32^3 \times 64$	[6, 32]	0.10454 (43)	0.05656 (37)
cB211.25.48		$48^3 \times 96$	[6, 48]	0.10454 (13)	0.05727 (11)
cB211.14.64		$64^3 \times 128$	[7, 64]	0.07845 (8)	0.05476 (12)
cB211.072.64		$64^3 \times 128$	[7, 64]	0.05659 (8)	0.05266 (15)
cC211.06.80	1.836	$80^3 \times 160$	[7, 80]	0.04721 (7)	0.04504 (10)

TABLE VII. *The time intervals $[t_{\min}, t_{\max}]$ adopted for the extraction of the pion mass and decay constant in lattice units obtained by applying the ODE method to the pion correlation function (14).*

Using the above pion data for f_π the NLO analysis of Section IV A, including the discretization term proportional to $a^2 M_\pi^2$, yields for the GF scale w_0 the value

$$w_0 = 0.1740 \text{ (16) fm} \quad (\text{B1})$$

in agreement with the result (52). Analogously, the use of the data for X_π and of the NLO fit (56) with $A'_2 = F_{FVE} = 0$ (see Section IV B) leads to

$$w_0 = 0.17389 \text{ (61) fm} \quad (\text{B2})$$

in agreement with the corresponding result shown in the second row of Table III.

Appendix C: Maximal twist corrections for masses and decay constants

We follow the general approach of Ref. [31] to the mixed action formulation of twisted mass lattice QCD, which ensures an unitary continuum limit (provided sea and valence

renormalized quark masses are matched). Here however we allow for small deviations (due e.g. to numerical errors) from the maximal twist case, i.e. for $m_0 \neq m_{cr}$.

1. $N_f=2+1+1$ isosymmetric QCD with twisted clover Wilson quarks

The lattice action can be conveniently written in terms of gauge, sea quark and valence quark plus valence ghost fields. If the sea quarks are arranged in two-flavour fields χ_ℓ and χ_h and the valence quarks are described by one-flavour fields χ_f , with $f = u, d, \dots$, we have

$$\begin{aligned} S = & S_g[U] + S_{\text{tm}}^\ell[\chi_\ell, \bar{\chi}_\ell, U; \mu_\ell, 0; m_0] + S_{\text{tm}}^h[\chi_h, \bar{\chi}_h, U; \mu_\sigma, \mu_\delta; m_0] \\ & + S_{\text{val}}[\{\chi_f, \bar{\chi}_f\}, U; \{\mu_f\}, m_0], \end{aligned} \quad (\text{C1})$$

with the valence sector given by

$$\begin{aligned} S_{\text{val}} = & \bar{\chi}_u[D_{W\text{clov}} + m_0 + i\mu_\ell\gamma_5]\chi_u + \bar{\chi}_d[D_{W\text{clov}} + m_0 - i\mu_\ell\gamma_5]\chi_d \\ & + \bar{\chi}_s[D_{W\text{clov}} + m_0 - i\mu_s\gamma_5]\chi_s + \bar{\chi}_c[D_{W\text{clov}} + m_0 + i\mu_c\gamma_5]\chi_c \\ & + \dots + \text{ghost terms}, \end{aligned} \quad (\text{C2})$$

where ellipses stand for possible replica (χ'_f) of the valence quarks with $\mu'_f = -\mu_f$ and the ghost terms exactly cancel the valence fermion contributions to the effective action. Here we find it convenient to express all fermion fields in the canonical quark basis for untwisted Wilson fermions and denote by $D_{W\text{clov}}$ the well-known clover improved (gauge covariant) Dirac matrix: $D_{W\text{clov}} = D_{W\text{clov}}[U] = \gamma \cdot \tilde{\nabla}[U] - (a/2)[\nabla^* \cdot \nabla][U] + i(c/4)\sigma \cdot F_{\text{clover}}[U]$.

We start by discussing the light valence quark sector, the extension to heavier flavours is straightforward. Following Refs. [28, 32], we define (as customary) the twist angle ω_ℓ in terms of the bare mass parameters of the *light valence quark* (u, d) doublet $X_\ell = (\chi_u, \chi_d)^T$, viz.

$$\sin \omega_\ell = \frac{\mu_\ell}{\sqrt{Z_A^2 m_{PCAC}^2 + \mu_\ell^2}}, \quad \cos \omega_\ell = \frac{Z_A m_{PCAC}}{\sqrt{Z_A^2 m_{PCAC}^2 + \mu_\ell^2}} \quad (\text{C3})$$

with Z_A the renormalization constant of $\bar{X}_\ell \gamma_\mu \gamma_5 (\tau^{1,2,3}/2) X_\ell$, which, being independent of quark mass parameters, is defined in the chiral limit $\mu_f \rightarrow 0$, $m_0 \rightarrow m_{cr}$. Maximal twist corresponds to $|\omega_\ell| = \pi/2$, i.e. to angle $\theta_\ell \equiv \pi/2 - \omega_\ell$ equal to zero or π . We thus have

$$\begin{aligned} \cos \theta_\ell = \sin \omega_\ell &= \frac{1}{\sqrt{1 + (Z_A^2 m_{PCAC}^2)/\mu_\ell^2}}, \\ \sin \theta_\ell = \cos \omega_\ell &= \frac{1}{\sqrt{1 + \mu_\ell^2/(Z_A^2 m_{PCAC}^2)}}. \end{aligned} \quad (C4)$$

Here μ_ℓ is the bare twisted mass parameters for the (u, d) doublet and m_{PCAC} denotes the untwisted bare quark mass of the (u, d) doublet as obtained from the non-singlet WTI's – hence a function of m_0 plus the other bare parameters. We recall that $m_{PCAC} \propto m_0 - m_{cr}$. The *renormalized* twisted and untwisted quark mass parameters that appear in the chiral WTI's read (up to discretization effects)

$$\mu_\ell^R = \mu_\ell \frac{1}{Z_P}, \quad m^R = Z_A m_{PCAC} \frac{1}{Z_P} = (m_0 - m_{cr}) \frac{1}{Z_{S^0}}, \quad (C5)$$

where Z_P and Z_{S^0} are the renormalization constants of the pseudoscalar non-singlet and the scalar singlet densities (in the canonical basis for untwisted Wilson quarks).

Defining the twist angle and hence formulating the maximal twist condition in terms of m_{PCAC} , as measured on the ensembles with 2+1+1 dynamical flavours, effectively takes care of (compensates for) all the UV cutoff effects related to the breaking of chiral symmetry, including those coming from the 2+1+1 sea quark flavours.

2. Pion mass and decay constant

We argue here that in the case of small enough numerical deviations from maximal twist the lattice charged pion quantities

$$M_\pi|_L, \quad [2\mu_\ell \langle \pi^1(\mathbf{0}) | P^1 | 0 \rangle / (M_\pi^2 \cos \theta_\ell)]|_L, \quad (C6)$$

with $P^1 = \bar{X}_\ell \gamma_5 (\tau^1/2) X_\ell$ and $X_\ell = (\chi_u, \chi_d)^T$, approach M_π and f_π as $a \rightarrow 0$ with lattice artifacts having numerically small, and (we shall see) within errors immaterial,

differences as compared to the $O(a^2)$ cutoff effects occurring at maximal twist. Of course these values of M_π and f_π correspond to the light quark renormalized mass $M_\ell^R = \sqrt{(m^R)^2 + (\mu_\ell^R)^2}$.

The numerical information on M_π and f_π comes from the simple correlator $C_{PP}^{11}(x_0) = a^3 \sum_{\mathbf{x}} \langle P^1(x) P^1(0) \rangle$ (and $C_{PP}^{22}(x_0)$). The large- x_0 behaviour of $C_{PP}^{11}(x_0)$ determines M_π and an exact lattice WTI relates the operator P^1 to the four-divergence of a *conserved lattice (backward one-point split) current*, which we denote by $\hat{V}_{\chi,\mu}^2$, v.i.z.

$$\partial_\mu \hat{V}_{\chi,\mu}^2(x) = 2\mu_\ell P^1(x) = 2\mu_\ell^R P_R^1(x), \quad (\text{C7})$$

implying that the pion-to-vacuum matrix element of $\hat{V}_{\chi,\mu}^2$ gives information on f_π (barring the case of $\cos \theta_\ell = 0$). In Eq. (C7) $P_R^1 = Z_P P^1$ and the equalities hold at operator level for finite lattice spacing ($a > 0$). Hence the l.h.s. of Eq. (C7) is a renormalized operator and information on the approach of its matrix elements to the continuum limit can be obtained by studying the behaviour as $a \rightarrow 0$ of the corresponding matrix elements of $2\mu_\ell^R P_R^1$.

Taking the matrix element of Eq. (C7) between the vacuum and a one- π^1 state of zero three-momentum and noting that in the continuum limit

$$\hat{V}_{\chi,\mu}^2 \xrightarrow{a \rightarrow 0} (\bar{X}_\ell \gamma_\mu (\tau^2/2) X_\ell)^R = \sin \theta_\ell \left(\bar{\psi} \gamma_\mu \frac{\tau^2}{2} \psi \right)^R + \cos \theta_\ell \left(\bar{\psi} \gamma_\mu \gamma_5 \frac{\tau^1}{2} \psi \right)^R, \quad (\text{C8})$$

where $\psi = (u, d)^T$ obeys the (continuum) e.o.m. $(\gamma \cdot D + M_\ell^R) \psi = 0$, for $a > 0$ one obtains

$$\begin{aligned} 2[\mu_\ell \langle \pi^1(\mathbf{0}) | P^1 | 0 \rangle]_L &= [\cos \theta_\ell M_\pi^2 f_\pi + \sin \theta_\ell \langle \pi^1(\mathbf{0}) | \partial_0 (\bar{\psi} \gamma_0 \frac{\tau^2}{2} \psi)^R | 0 \rangle]_L \\ &= [\cos \theta_\ell M_\pi^2 f_\pi]_L + O(a). \end{aligned} \quad (\text{C9})$$

This relation implies that as $a \rightarrow 0$ the ratio

$$[2\mu_\ell \langle \pi^1(\mathbf{0}) | P^1 | 0 \rangle / (M_\pi^2 \cos \theta_\ell)]_L \rightarrow f_\pi, \quad (\text{C10})$$

at generic $\theta_\ell \neq \pm\pi/2$. Hence at $a > 0$ the ratio (C10) represents a *bona fide* lattice estimator of f_π , while its discretization errors depend on the lattice artifacts in M_π^2 , θ_ℓ (or equivalently m^R , μ_ℓ^R) and the renormalized quantity $2\mu_\ell G_{\pi^1} = 2\mu_\ell \langle \pi^1(\mathbf{0}) | P^1 | 0 \rangle$.

We are interested here in situations where $Z_{Am_{PCAC}}/\mu_\ell < 1$ but not negligibly small, say slightly above 0.1. This situation indeed occurs in our gauge configuration ensemble cA211.12.48, at $a \sim 0.095$ fm and $a\mu_\ell = 0.0012$, where we find $Z_{Am_{PCAC}}/\mu_\ell \sim -0.15$. In this case an analysis à la Symanzik of M_π^2 , m_ℓ^R and $2\mu_\ell G_{\pi^1}$ shows (see below) that the change in the lattice artifacts of our lattice estimator of f_π , with respect to those purely $O(a^{2n})$ (with n integer) that occur at maximal twist, is smaller than $0.001f_\pi$, therefore numerically immaterial within statistical errors that are typically of order $0.005f_\pi$.

a. The change in the lattice artifacts for M_π^2 and f_π

If $|am_{PCAC}|$ is non-zero, though definitely smaller than $|a\mu_\ell|$, the same holds for $|a(m_0 - m_{cr})|$ and one expects that the appropriate lattice estimators of M_π , f_π and any other physical quantity will be altered already at $O(a)$ as compared to their counterparts at maximal twist. Correcting analytically the lattice estimators for the deviation from maximal twist at order a^0 is hence not enough and one must also check that the out-of-maximal-twist modifications in order a and order a^2 lattice artifacts are numerically negligible within statistical errors. Otherwise, analysing data corrected for deviations from maximal twist on some gauge ensembles together with data evaluated at maximal twist on other gauge ensembles might lead to a systematic bias in the continuum extrapolation, where one typically assumes uniform $O(a^2)$ artifacts – as expected if all data are obtained at maximal twist.

b. Structure of the Symanzik effective Lagrangian

Let us analyse à la Symanzik the $N_f = 2 + 1 + 1$ lattice QCD theory (C1) out-of-maximal-twist and focus here on the light valence sector. We assume the reader is familiar with the basic literature on this topic such as [28, 56, 57] and references therein. The Symanzik local effective Lagrangian (LEL) to be used in our analysis of

$O(a)$ artifacts then reads

$$\begin{aligned}
L_{Syma} &= L_4 + aL_5 + a^2L_6 + O(a^3) , \\
L_4 &= \frac{1}{4}(F \cdot F) + \bar{\chi}_\ell (\gamma \cdot D + m^R + i\gamma_5 \tau^3 \mu_\ell^R) \chi_\ell \\
&\quad + \bar{\chi}_h (\gamma \cdot D + m^R + i\gamma_5 \tau^3 \mu_h + \tau^1 \epsilon_h) \chi_h \\
&\quad + \bar{X}_\ell^{val} (\gamma \cdot D + m^R + i\gamma_5 \tau^3 \mu_\ell^R) X_\ell^{val} + \dots , \tag{C11}
\end{aligned}$$

where $X_\ell^{val} = (\chi_u, \chi_d)^T$ describes the valence light quarks in the same basis as in Eq. (C2) while ellipses stands for $d \leq 4$ terms involving heavier valence quarks and ghost terms. Upon taking the continuum limit in isosymmetric QCD with 2+1+1 dynamical flavours, we must have coinciding sea and valence renormalized masses for each flavour and keep constant as $a \rightarrow 0$ the renormalized parameters g_R^2 , μ_ℓ^R , μ_h^R , ϵ_h^R .

The LEL terms L_n are suitable linear combinations of the $d = n > 4$ operator terms allowed by the symmetries of the lattice theory (C1). In particular it turns out that

$$\begin{aligned}
L_5 &= \dots + (c - c_{SW}) \frac{i}{4} \bar{X}_\ell^{val} \sigma \cdot F X_\ell^{val} - b_g m \frac{1}{4} F \cdot F \\
&\quad - (b_m m^2 + \tilde{b}_m \mu_\ell^2) \bar{X}_\ell^{val} X_\ell^{val} - b_\mu m \mu_\ell \bar{X}_\ell^{val} i\gamma_5 \tau^3 X_\ell^{val} + \dots , \tag{C12}
\end{aligned}$$

where $m \equiv Z_{AMPAC} \propto m_0 - m_{cr}$, while ellipses stand here for terms involving only heavier valence quark operators as well as sea quark and ghost terms (all of them are omitted since they are immaterial for this Section). With $c - c_{SW}$ we indicate the difference between the 1-loop tadpole improved estimate (c) employed in our simulation and the exact value (c_{SW}) of the coefficient of the clover term³.

Concerning L_6 , it will be enough to focus on its m -dependent sector and to note the structure

$$L_6(m; \mu_\ell, \mu_h, \epsilon_h, \mu_s, \dots) = L_6(0; \mu_\ell, \mu_h, \epsilon_h, \mu_s, \dots) + mO_5 + m^2O_4 , \tag{C13}$$

³ From our experience in simulations with two dynamical flavours in a lattice setup where c_{SW} is known, we expect that $|c - c_{SW}| < 0.15$, which suppresses $O(a)$ lattice artifact by nearly one order of magnitude and, provided $|am/a\mu_\ell| < 1$ is small enough, makes undesired $O(a)$ numerically negligible in most observables.

where O_5 (O_4) is a linear combination of the m -independent terms allowed in L_5 (L_4). Among the latter, since we employ in our correlators flavour diagonal OS valence quark fields χ_f^{val} with twisted mass $\mu_f > 0$, or $\chi_f^{\prime val}$ fields with twisted mass $\mu_f' = -\mu_f$, for the purposes of this Section only the terms bilinear in the X_ℓ^{val} and \bar{X}_ℓ^{val} , or $X_\ell^{\prime val}$ and $\bar{X}_\ell^{\prime val}$, fields are relevant, which we may call $mO_{5,\ell}^{val}$ and $m^2O_{4,\ell}^{val}$.

We note that exact or spurionic lattice symmetries rule out ⁴ the L_5 terms of the form

$$\mu_f i\tilde{F}\cdot F, \quad \mu_f \bar{X}_f \tau^{0,1,2,3} i\gamma_5 \gamma \cdot DX_f, \quad \mu_f \bar{X}_f \tau^{0,1,2,3} \gamma \cdot DX_f,$$

as well as the analogous L_6 terms of the form

$$m\mu_f i\tilde{F}\cdot F, \quad m\mu_f \bar{X}_f \tau^{0,1,2,3} i\gamma_5 \gamma \cdot DX_f, \quad m\mu_f \bar{X}_f \tau^{0,1,2,3} \gamma \cdot DX_f.$$

c. The discretization effects on $M_\pi|_L$

In the case of $|am| \sim 0.0002 < |a\mu_\ell| = 0.0012$, for the quantity $M_\pi^2|_L$ the $O(a)$ deviation from its continuum limit value $M_\pi^2 = 2B^R \sqrt{(m^R)^2 + (\mu_\ell^R)^2} + O((m^R)^2 + (\mu_\ell^R)^2) \sim 2B^R \mu_\ell^R$ is given by

$$\delta_1 M_\pi^2 = \delta_{1A} M_\pi^2 + \delta_{1B} M_\pi^2, \quad (\text{C14})$$

where, writing operators in terms of the physical basis fermion doublet fields

$$\psi_\ell = e^{i\omega_\ell \gamma_5 \tau^3 / 2} X_\ell, \quad \bar{\psi}_\ell = \bar{X}_\ell e^{i\omega_\ell \gamma_5 \tau^3 / 2}$$

and exploiting parity and isospin symmetries of continuum $N_f = 2 + 1 + 1$ QCD, one has

$$\begin{aligned} \delta_{1A} M_\pi^2 &= a \sin \theta_\ell \langle \pi^{1,2}(\mathbf{0}) | (c - c_{SW}) \bar{\psi}_\ell^{val} \frac{i}{4} \sigma \cdot F \psi_\ell^{val} - (b_m m^2 + \tilde{b}_m \mu_\ell^2) \bar{\psi}_\ell^{val} \psi_\ell^{val} | \pi^{1,2}(\mathbf{0}) \rangle \\ &\lesssim 0.003 \frac{\alpha_s(\Lambda_{QCD})}{4\pi} \Lambda_{QCD}^2 \sim 0.001 M_\pi^2 \end{aligned} \quad (\text{C15})$$

⁴ To this goal it is enough to consider charge combination, $\tilde{P} \times (\mu_{f,\ell,h} \rightarrow -\mu_{f,\ell,h})$ and $(X_f \rightarrow i\tau^2 X_f) \times (\bar{X}_f \rightarrow -i\bar{X}_f \tau^2) \times (\mu_{f,\ell,h} \rightarrow -\mu_{f,\ell,h})$ invariances, with \tilde{P} meaning parity transformation on gauge fields combined with $(X_f(x) \rightarrow \gamma_0 X_f(x_P)) \times (\bar{X}_f(x) \rightarrow \bar{X}_f(x_P) \gamma_0)$ and $x_P = (x_0, -\vec{x})$.

and (approximating $\cos \theta_\ell$ with 1, since $\sin \theta_\ell \simeq 0.2$)

$$\begin{aligned} \delta_{1B} M_\pi^2 &= am \langle \pi^{1,2}(\mathbf{0}) | (b_\mu \mu_\ell \bar{\psi}_\ell^{val} \psi_\ell^{val} + b_g \frac{1}{4} F \cdot F) | \pi^{1,2}(\mathbf{0}) \rangle \\ &\lesssim 2B^R \mu_\ell^R 0.0005. \end{aligned} \quad (\text{C16})$$

The numerical estimate in Eq. (C15) results from $|c - c_{SW}| \lesssim 0.15$, $\alpha_s(\Lambda_{QCD}) \sim 1$, $a\Lambda_{QCD} \simeq 0.1$ and $\Lambda_{QCD}/M_\pi \simeq 2$, while $b_m = -1/2 + O(g_0^2)$ and (making the choice advocated in Ref. [57]) $\tilde{b}_\mu = -1/2$.

The numerical estimate in Eq. (C16) follows from $|\langle \pi^{1,2}(\mathbf{0}) | \mu_\ell \bar{\psi}_\ell^{val} \psi_\ell^{val} | \pi^{1,2}(\mathbf{0}) \rangle| \sim |2B^R \mu_\ell^R|$ and $|b_\mu| = O(g_0^2) < 1$. In fact soft pion theorems (i.e. spontaneously broken continuum chiral symmetry) imply that the contribution of $|b_g \langle \pi^{1,2}(\mathbf{0}) | \frac{1}{4} F \cdot F | \pi^{1,2}(\mathbf{0}) \rangle|$, with $b_g = O(g_0^2 N_f)$, is $O(\mu_\ell)$ and thus of the same order of magnitude as $|b_\mu \langle \pi^{1,2}(\mathbf{0}) | \mu_\ell \bar{\psi}_\ell^{val} \psi_\ell^{val} | \pi^{1,2}(\mathbf{0}) \rangle|$.

The undesired $O(a)$ modification in M_π^2 is estimated to be smaller than $0.001 M_\pi^2$, hence immaterial within our statistical errors of a few permil. The $O(a^2)$ change in M_π^2 due to the non-zero value of am is also of order $0.001 M_\pi^2$ or smaller, because of the form (C13) of L_6 , with $|am| \simeq 0.0002$ and $a^2 \Lambda_{QCD}^2 \sin \theta_\ell \simeq 0.001$.

d. The discretization effects on $f_\pi|_L$

Based on Eq. (C10) the lattice artifacts on f_π can be estimated in terms of the cutoff effects in $(\mu_\ell / \cos \theta_\ell) \langle \pi^1(\mathbf{0}) | P^1 | 0 \rangle|_L$ and in $M_\pi^2|_L$. We discussed above the lattice artifacts of $M_\pi^2|_L$. Concerning $(\mu_\ell / \cos \theta_\ell) \langle \pi^1(\mathbf{0}) | P^1 | 0 \rangle|_L$, we can see it as the product of the renormalized quantities $Z_P^{-1}(\mu_\ell / \cos \theta_\ell) = M_\ell^R$ and $Z_P \langle \pi^1(\mathbf{0}) | P^1 | 0 \rangle|_L = G_{\pi^1}^R$, and then discuss separately the lattice artifacts in each of these two factors⁵.

As for $Z_P^{-1}(\mu_\ell / \cos \theta_\ell) = \sqrt{(m^R)^2 + (\mu_\ell^R)^2}$, the form of the m -dependent terms in L_5 , i.e. those with coefficients b_m and b_μ (which are all in modulus $\lesssim 1$), implies that the $O(a)$

⁵ Of course we do not worry about possible cutoff effects on Z_P , which cancel in the product.

corrections to m^R and μ_ℓ^R , and hence to M_ℓ^R are only of relative size $< |am| \simeq 0.0002$. Even smaller are the corrections to M_ℓ^R of order a^2m .

Let us then consider the out-of-maximal-twist induced cutoff artifacts in the matrix element $Z_P \langle \pi^1(\mathbf{0}) | P^1 | 0 \rangle | L = G_{\pi^1}^R$. They clearly arise from the lattice two-point correlator $C_P^{11}(x_0)$. At order a , since for the operator $P^1 = \bar{\psi}_\ell \gamma_5 (\tau^1/2) \psi_\ell$ it is known that $c_P = 0$, $\tilde{b}_P = 0$ and $b_P = 1 + O(g_0^2)$, implying $|b_P am| \sim 0.0002$, the numerically dominant lattice artifacts stem from the term $a \int d^4y \langle P^1(x) P^1(0) L_5(y) \rangle |_{\text{cont}}$ in the Symanzik description of $C_{11}(x_0)$. Inserting intermediate states and considering the possible y_0 -orderings one checks that, owing to the structure of L_5 and $|am| \simeq 0.0002$, the numerically leading cutoff effects in G_{π^1} are proportional to

$$(c - c_{SW}) \sin \theta_\ell a \left[\langle \pi^1 | \bar{\psi}_\ell^{val} \frac{i}{4} \sigma \cdot F \psi_\ell^{val} | \pi^1 \rangle G_{\pi^1} + \sum_n \langle 0 | \bar{\psi}_\ell^{val} \frac{i}{4} \sigma \cdot F \psi_\ell^{val} | n \rangle \langle n | P^1 | \pi^1 \rangle \right]$$

and are hence of relative order $|\sin \theta_\ell (c - c_{SW})| a \Lambda_{QCD} \alpha_s / (4\pi)$, which, if $|am| \simeq 0.0002$ and $|c - c_{SW}| < 0.15$, noting that $a \Lambda_{QCD} \alpha_s / (4\pi) < 0.1$, turns out to be $\lesssim 0.0002$. Compared to this the $O(a^2m)$ artifacts in G_{π^1} are expected to be smaller by at least one order of magnitude.

Hence our lattice estimator of f_π is estimated to be affected by the small deviation from maximal twist observed on the ensemble cA211.A12.48, where $|am| \sim 0.0002$, only at a level of $\lesssim 0.0004 f_\pi$, which is negligible as compared to current statistical errors.

e. Analysis of M_π^2 and f_π in terms of the renormalized light quark mass

The discussion above is valid also in case the observables M_π^2 and f_π are analysed as functions of the renormalized light quark mass

$$M_\ell^R = \sqrt{(m^R)^2 + (\mu_\ell^R)^2} = Z_P^{-1}(\mu_\ell / \cos \theta_\ell). \quad (\text{C17})$$

As already noted in Section C2d, for the ensemble cA211.12.48 the observed small deviation from maximal twist leads to an undesired $O(am)$ relative change in M_ℓ^R that is only of order $|am| \simeq 0.0002$ and thus fully negligible in comparison to other errors.

A rather obvious but practically important and general caveat follows in the case one insists in analysing the lattice data, e.g. for M_π or f_π , obtained on gauge ensembles with non-zero am -values in terms of μ_ℓ^R rather than M_ℓ^R . Since for $am \neq 0$ a generic observable Q_{obs} actually refers to $M_\ell^R > \mu_\ell^R$, one should, besides possibly applying an analytic correction to the datum for Q_{obs} (as requested e.g. for f_π , but not for M_π), also shift the value of the observable itself according to

$$Q_{obs}(\mu_\ell^R) = Q_{obs}(M_\ell^R) + \left. \frac{\partial Q_{obs}}{\partial M_\ell^R} \right|_{M_\ell^R} (\mu_\ell^R - M_\ell^R) + \mathcal{O}((\mu_\ell^R - M_\ell^R)^2), \quad (\text{C18})$$

where in practice, since typically $|am| < 0.001$, only the terms linear in $\mu_\ell^R - M_\ell^R$ are numerically important.

3. Mass and decay constant of the kaon and heavier PS-mesons

Generalizing the arguments of Section C 2 for the mass and decay constant of the pion to the case of the kaon or heavier pseudoscalar (PS) mesons is rather straightforward. Indeed, within the $N_f = 2 + 1 + 1$ lattice QCD framework of Section C 1, as far as the control of the effects of a small but non-zero value of $am = aZ_{AMPAC}$ is concerned, there is not much difference between a PS meson made out of two light valence quarks (pion, with $|\mu_u| = |\mu_d|$) and a PS meson made out of a light (mass μ_ℓ) and a heavier (mass μ_x) valence quark. This is a consequence of the fact that the extraction of the PS meson mass and decay constant relies on general positivity properties of two-point correlation functions (close enough to the continuum limit) and on exact chiral WTI's, which hold valid irrespectively of the value of valence quark masses. One might thus deal in a fully analogous way with PS mesons made out of two non-light valence quarks. For definiteness, however, we shall here focus on the case of the kaon, i.e. $\mu_x = \mu_s \gg \mu_\ell$ and $\mu_d = \mu_\ell > 0$.

It turns out that in the case of small enough numerical deviations from maximal twist, say $0.1 a\mu_\ell < |am| \ll a\mu_\ell \ll a\mu_s$, the lattice charged kaon quantities

$$M_K|_L, \quad [(\mu_\ell + \mu_s)\langle K(\mathbf{0})|P^{s,d}|0\rangle / (M_K^2 \cos((\theta_\ell + \theta_s)/2))]|_L, \quad (\text{C19})$$

with $P^{s,d} = \bar{X}_{s,d}\gamma_5(\tau^1/2)X_{s,d}$ and $X_{s,d} = (\chi_s, \chi_d)^T$, approach M_K and f_K as $a \rightarrow 0$ with lattice artifacts having numerically small, and within errors immaterial, differences as compared to the $O(a^2)$ cutoff effects occurring at maximal twist. These values of M_K and f_K correspond to the light (d) quark renormalized mass $M_\ell^R = \sqrt{(m^R)^2 + (\mu_\ell^R)^2}$ and to the strange (s) quark renormalized mass $M_s^R = \sqrt{(m^R)^2 + (\mu_s^R)^2}$.

In full analogy to the definitions adopted for light valence quarks (see Section C 1) we define $\mu_s^R = \mu_s/Z_P$, where Z_P is (can be conveniently taken as) the same mass-independent renormalization constant of the PS non-singlet quark bilinear operator as above, and

$$\begin{aligned} \cos \theta_s = \sin \omega_s &= \frac{1}{\sqrt{1 + (Z_A^2 m_{PCAC}^2)/\mu_s^2}}, \\ \sin \theta_s = \cos \omega_s &= \frac{1}{\sqrt{1 + \mu_s^2/(Z_A^2 m_{PCAC}^2)}}. \end{aligned} \quad (\text{C20})$$

a. On the lattice estimators (C19) of M_K and f_K at $O(a^0)$

The numerical information on M_K and f_K comes in fact from the simple correlator $C_{KK}^{s,d}(x_0) = a^3 \sum_{\mathbf{x}} \langle P^{s,d}(x) P^{d,s}(0) \rangle$. The large- x_0 behaviour of $C_{KK}^{s,d}(x_0)$ determines M_K as the kaon mass that, owing to renormalizability (and unitarity in the continuum limit) of the lattice theory of Section C 1, corresponds to the light and strange quark masses M_ℓ^R and M_s^R . An exact lattice WTI relates the operator $P^{s,d}$ to the four-divergence of a conserved lattice (backward one-point split) current, which we denote by $\hat{V}_{\chi,\mu}^{s,d}$, viz.

$$\partial_\mu \hat{V}_{\chi,\mu}^{s,d}(x) = (\mu_\ell + \mu_s) P^{s,d}(x) = (\mu_\ell^R + \mu_s^R) P_R^{s,d}(x), \quad (\text{C21})$$

implying that the kaon-to-vacuum matrix element of $\hat{V}_{\chi,\mu}^{s,d}$ gives information on f_K , barring the case of $\cos((\theta_\ell + \theta_s)/2) = 0$. In Eq. (C21) $P_R^{s,d} = Z_P P^{s,d}$ and the equalities hold at operator level for $a > 0$. Hence the l.h.s. of Eq. (C21) is a renormalized operator and information on the approach of its matrix elements to the continuum limit can be obtained by studying the behaviour as $a \rightarrow 0$ of the corresponding matrix elements of $(\mu_\ell^R + \mu_s^R) P_R^{s,d}$.

Taking the matrix element of Eq. (C21) between the vacuum and a one- K state of zero three-momentum and noting that in the continuum limit

$$\begin{aligned} \hat{V}_{\chi,\mu}^{s,d} \xrightarrow{a \rightarrow 0} (\bar{X}_{s,d} \gamma_\mu (\tau^2/2) X_{s,d})^R &= \sin \frac{\theta_\ell + \theta_s}{2} \left(\bar{\psi}_{s,d} \gamma_\mu \frac{\tau^2}{2} \psi_{s,d} \right)^R \\ &+ \cos \frac{\theta_\ell + \theta_s}{2} \left(\bar{\psi} \gamma_\mu \gamma_5 \frac{\tau^1}{2} \psi \right)^R, \end{aligned} \quad (\text{C22})$$

where $\psi_{s,d} = (s, d)^T$ obeys the (continuum) e.o.m. $(\gamma \cdot D + \frac{M_s^R + M_\ell^R}{2} + \frac{M_s^R - M_\ell^R}{2} \tau^3) \psi_{s,d} = 0$, for $a > 0$ one obtains

$$[(\mu_\ell + \mu_s) \langle K(\mathbf{0}) | P^{s,d} | 0 \rangle]_L = [\cos((\theta_\ell + \theta_s)/2) M_K^2 f_K]_L + O(a). \quad (\text{C23})$$

This relation implies that as $a \rightarrow 0$ the ratio

$$[(\mu_\ell + \mu_s) \langle K(\mathbf{0}) | P^{s,d} | 0 \rangle / (M_K^2 \cos((\theta_\ell + \theta_s)/2))]_L \rightarrow f_K, \quad (\text{C24})$$

for generic $\theta_\ell + \theta_s \neq \pm\pi$. Hence at $a > 0$ the ratio (C24) represents a *bona fide* lattice estimator of f_K , while its discretization errors depend on the lattice artifacts in M_K^2 , θ_ℓ , θ_s (or equivalently m^R , μ_ℓ^R , μ_s^R) and the renormalized quantity $(\mu_\ell + \mu_s) G_K = (\mu_\ell + \mu_s) \langle K(\mathbf{0}) | P^{s,d} | 0 \rangle$.

b. Theoretical control and numerical size of $O(a)$ and $O(a^2)$ artifacts

Concerning the impact of a non-zero am value on the lattice artifact in the kaon sector it is important to note that, as phenomenology dictates $\mu_\ell \simeq 0.037\mu_s$, we have in general

$$\begin{aligned} \theta_s \ll \theta_\ell, \quad \cos((\theta_\ell + \theta_s)/2) &\simeq \cos(\theta_\ell/2) [1 - O(\theta_s^2)] - O(\theta_s \theta_\ell) \\ &\simeq \cos(\theta_\ell/2) - O(\theta_s \theta_\ell). \end{aligned} \quad (\text{C25})$$

In particular, for the gauge ensemble cA211.12.48, where $am = Z_{AMPAC}/\mu_l \simeq -0.15$, we find

$$\theta_\ell \simeq -0.15, \quad \theta_s \simeq -0.006, \quad \cos((\theta_\ell + \theta_s)/2) \simeq \cos(\theta_\ell/2) - O(0.0009). \quad (\text{C26})$$

For the discussion of $O(a)$ lattice artifacts in M_K and f_K one should consider of course the occurrence of flavour diagonal terms involving the valence quark fields $\chi_s, \bar{\chi}_s$ both in L_5 (see Eq. (C12)), where they take the form

$$L_5 \supset (c - c_{SW}) \frac{i}{4} \bar{\chi}_s^{val} \sigma \cdot F \chi_s^{val} - (b_m m^2 + \tilde{b}_m \mu_s^2) \bar{\chi}_s^{val} \chi_s^{val} - b_\mu m \mu_s \bar{\chi}_s^{val} i \gamma_5 \chi_s^{val}, \quad (\text{C27})$$

and in L_6 , for which the structure in Eq. (C13) remains valid. Looking back to Eq. (C12) for the light valence quark and gluonic terms in L_5 , one finds that the discussion for the kaon case closely follows the one for the pion (see Section C2a), provided one replaces the valence quark field pair $X_\ell^{val} = (\chi_u, \chi_d)^T$, used for the latter, with the valence quark field pair $X_{s,d}^{val} = (\chi_s, \chi_d)^T$ relevant for the kaon, as well as θ_ℓ with $(\theta_s + \theta_\ell)/2$. This implies that for M_K^2 and f_K the numerically dominant changes in the lattice artifacts as compared to the maximal twist case, which for M_π^2 and f_π were proportional to $\sin \theta_\ell$, turn out to be proportional to

$$\sin((\theta_\ell + \theta_s)/2) \simeq \sin(\theta_\ell/2) - O(0.006) \simeq 0.5 \sin \theta_\ell, \quad (\text{C28})$$

thereby getting reduced by a factor of about two with respect to the pion case.

In conclusion, if $|am| \sim 0.0002$ (as it happens for our ensemble cA211.12.48), we estimate a lattice artifact modification, with respect to the case of maximal twist, that does not exceed $0.0005 M_K^2$ for M_K^2 and $0.0002 f_K$ for f_K and is hence safely negligible as compared to our current statistical errors.

From the arguments above it should also be clear that the same quantitative estimates hold also for the lattice artifact changes induced by $am \neq 0$ in the mass and the decay constant of heavy-light PS mesons with a charm or even heavier non-light valence quark having a mass $\mu_x \gg \mu_s$. In fact the heavier the valence quark, the smaller $|\theta_x| \simeq |m/\mu_x|$ and the more numerically irrelevant the effect of a small non-zero value of am .

Appendix D: Determination of the GF scales $\sqrt{t_0}$ and t_0/w_0

In this Appendix we describe the calculations of the relative GF scales $w_0/a, \sqrt{t_0}/a$ and $t_0/(w_0 a)$ at the physical pion point and we summarize the determination of the

absolute scales $\sqrt{t_0}$ and t_0/w_0 using the SU(2) ChPT analysis of the data for X_π , carried out in Section IV B in the case of the GF scale w_0 .

1. Determination of the relative GF scales

In this section we provide the details of the determinations of the gradient flow (GF) scales at the physical point. Our analysis is based on the values of the gradient flow scales in Table VIII as obtained on the ensembles in Table I. We calculate the scales following the definitions in [13, 14, 58] using the standard Wilson action for the gradient flow evolution and the symmetrized discretization of the action density as described in [14]. Apart from the usual scales $s_0/a \equiv \sqrt{t_0}/a$ and w_0/a , we also consider the derived scale $(t_0/w_0)/a$ as well as the dimensionless ratio (s_0/w_0) . The former is interesting, because it exhibits very mild quark-mass dependence and reduced autocorrelations, while the dimensionless ratio (s_0/w_0) can be used for assessing lattice artefacts and crosschecking the consistency of the various analysis procedures and determinations of the scales in physical units.

The errors are calculated by taking into account the autocorrelations of the various quantities, which are also listed in Table VIII. It is well known that the autocorrelations can be sizable for the GF scales. In particular on coarse lattices it is known that they can be larger than the ones for the topological charge [59]. More importantly, they are also expected to grow towards the chiral limit. The data shown in Table VIII confirms this behaviour in terms of the lattice spacing and the pion mass. The large autocorrelations observed on the ensemble cA211.12.48, corresponding to the coarsest lattice spacing and the smallest pion mass, could be also related to metastability effects known for this ensemble. Nonetheless, the data in Table VIII also indicates that for our simulations the autocorrelations are well under control even at the physical point. One interesting point to note is the fact that the autocorrelations of the scale $(t_0/w_0)/a$ are reduced by roughly a factor 3 with respect to the ones of the usual GF scales $\sqrt{t_0}/a$ and w_0/a . This is also reflected in the very small statistical error for $(t_0/w_0)/a$, roughly a factor

ensemble	N_{meas}	s_0/a	w_0/a	$(t_0/w_0)/a$	s_0/w_0	$\tau_{\text{int}}^{s_0}$	$\tau_{\text{int}}^{w_0}$	$\tau_{\text{int}}^{t_0/w_0}$	$\tau_{\text{int}}^{s_0/w_0}$
cA211.53.24	1122	1.5306(21)	1.7597(43)	1.33139(89)	0.86982(100)	23(6)	25(7)	7(1)	18(4)
cA211.40.24	1219	1.5384(18)	1.7766(33)	1.33213(96)	0.86592(64)	20(5)	18(4)	7(1)	9(2)
cA211.30.32	2559	1.5460(9)	1.7928(17)	1.33314(47)	0.86233(32)	22(5)	21(4)	9(1)	10(2)
cA211.12.48	326	1.5614(22)	1.8249(33)	1.33590(155)	0.85559(29)	69(30)	63(27)	59(25)	16(5)
cB211.25.24	1145	1.7937(22)	2.0992(46)	1.53260(108)	0.85445(77)	21(5)	25(6)	5(1)	12(2)
cB211.25.32	990	1.7922(19)	2.0991(47)	1.53018(72)	0.85380(91)	35(10)	45(14)	6(1)	28(7)
cB211.25.48	1175	1.7915(8)	2.0982(19)	1.52966(41)	0.85384(38)	28(8)	31(9)	9(2)	20(5)
cB211.14.64	619	1.7992(5)	2.1175(11)	1.52875(23)	0.84968(23)	30(8)	32(9)	8(1)	23(6)
cB211.072.64	191	1.8028(8)	2.1272(19)	1.52784(42)	0.84750(41)	45(18)	52(22)	16(5)	41(16)
cC211.06.80	785	2.1094(8)	2.5045(17)	1.77670(37)	0.84226(27)	46(17)	42(16)	14(3)	26(8)

TABLE VIII. GF scales and corresponding integrated autocorrelation times in units of trajectories of length $\tau = 1.0$ from the symmetrized action density. The N_{meas} measurements on different ensembles were performed using different separations and the autocorrelation times were scaled appropriately. Similarly, for the cB211.25.24, cB211.25.32 and cB211.14.64 ensembles, the autocorrelation times were scaled to take into account the $\tau = 1.5$ trajectory lengths used there.

2-3 smaller than for $\sqrt{t_0}/a$ and w_0/a at the physical point.

In order to use the scales in the analysis of the light meson sector, we need the values at the physical pion-mass point. To achieve this, we perform an extrapolation for the two sets of ensembles cA211 and cB211⁶ to the physical point in terms of $\Delta^2 \equiv (M_\pi/f_\pi)^2 - (M_\pi/f_\pi)_{\text{phys.}}^2$, such that the physical point is reached when this quantity is zero, while for the ensemble cC211.06.80 we directly use the value at the physical point as given in Table VIII. We note that for this ensemble $\Delta^2 = 0.025$ such that the potential corrections would be tiny and in fact smaller than the statistical errors. The details of the extrapolations are summarized in Table IX. In order to illustrate the extrapolations and compare them at different lattice spacings, in Fig. 10 we show the scales normalized by their values at the physical point as a function of Δ^2 .

From the plots and the data in the table it is obvious that the quark-mass dependence

⁶ The results for the ensembles cB211.25.24 and cB211.25.32 shown in Table VIII are not used for the determination of the relative GF scales at the physical pion point, since finite-volume effects are found to be negligible with respect to the other uncertainties for $M_\pi L \gtrsim 3.5$ (see also Table I).

	$(s_0/a)_{\text{phys.}}$	c	$\chi^2/\text{d.o.f.}$	$(w_0/a)_{\text{phys.}}$	c	$\chi^2/\text{d.o.f.}$
cA211	1.5660(22)	-0.0082(8)	0.02	1.8352(35)	-0.0174(13)	0.00
cB211	1.80396(68)	-0.0053(5)	2.14	2.1299(16)	-0.0136(12)	1.84

	$((t_0/w_0)/a)_{\text{phys.}}$	c	$\chi^2/\text{d.o.f.}$	$(s_0/w_0)_{\text{phys.}}$	c	$\chi^2/\text{d.o.f.}$
cA211	1.3359(12)	-0.0011(4)	0.15	0.8531(10)	0.0038(4)	0.05
cB211	1.52789(33)	0.0008(3)	0.18	0.84697(37)	0.0030(3)	1.26

TABLE IX. Results for the extrapolations of the GF scales to the physical point in terms of $\Delta^2 = (M_\pi/f_\pi)^2 - (M_\pi/f_\pi)_{\text{phys.}}^2$, i.e., $X(M_\pi)/a = (X/a)_{\text{phys.}} + c \cdot \Delta^2$. Note that for the ensembles cA211 we have $N_{\text{d.o.f.}} = 2$, while for cB211 $N_{\text{d.o.f.}} = 1$.

of the scale $(t_0/w_0)/a$ is very small, i.e., the corrections are less than 0.5% at our largest pion mass ensemble cA211.53.24, to be compared to 2.5% for $\sqrt{t_0}/a$ and 4.5% for w_0/a . We note that the quark-mass dependence exhibits clearly visible lattice artefacts, but the dependence seems to become weaker towards the continuum limit. One peculiar feature is the fact that for the scale $(t_0/w_0)/a$ the slope of the quark-mass dependence changes sign when going from the coarser to the finer lattice spacing. This certainly warrants further investigation, once more data is available, however, one should keep in mind that for this quantity the slope is consistent with zero within less than 3σ .

In order to examine the lattice artefacts of the GF scales further, we now turn to the dimensionless ratio s_0/w_0 . In Figure 11 we show the ratio at the physical point as a function of the lattice spacing expressed in units of the three GF scales $s_0^{\text{phys.}}$, $w_0^{\text{phys.}}$ and $t_0^{\text{phys.}}/w_0^{\text{phys.}}$ at the physical point. Note that for the lattice spacing cC211 this corresponds to the value obtained on the ensemble cC211.06.680. The data show a precise $\mathcal{O}(a^2)$ -scaling towards the continuum and allow continuum extrapolations in terms of a^2 . The continuum extrapolations using in turn $a^2/(t_0/w_0)^2$, a^2/t_0 and a^2/w_0^2 yield $(s_0/w_0)^{\text{phys.}} = 0.8285(13)$, $0.8291(13)$ and $0.8298(12)$, respectively, with $\chi^2/\text{d.o.f.} = 0.20$, 0.12 and 0.06 . The values in the continuum are perfectly consistent with each other and averaging them in the usual way gives $(s_0/w_0)^{\text{phys.}} = 0.8291(13)(5)[14]$, where the

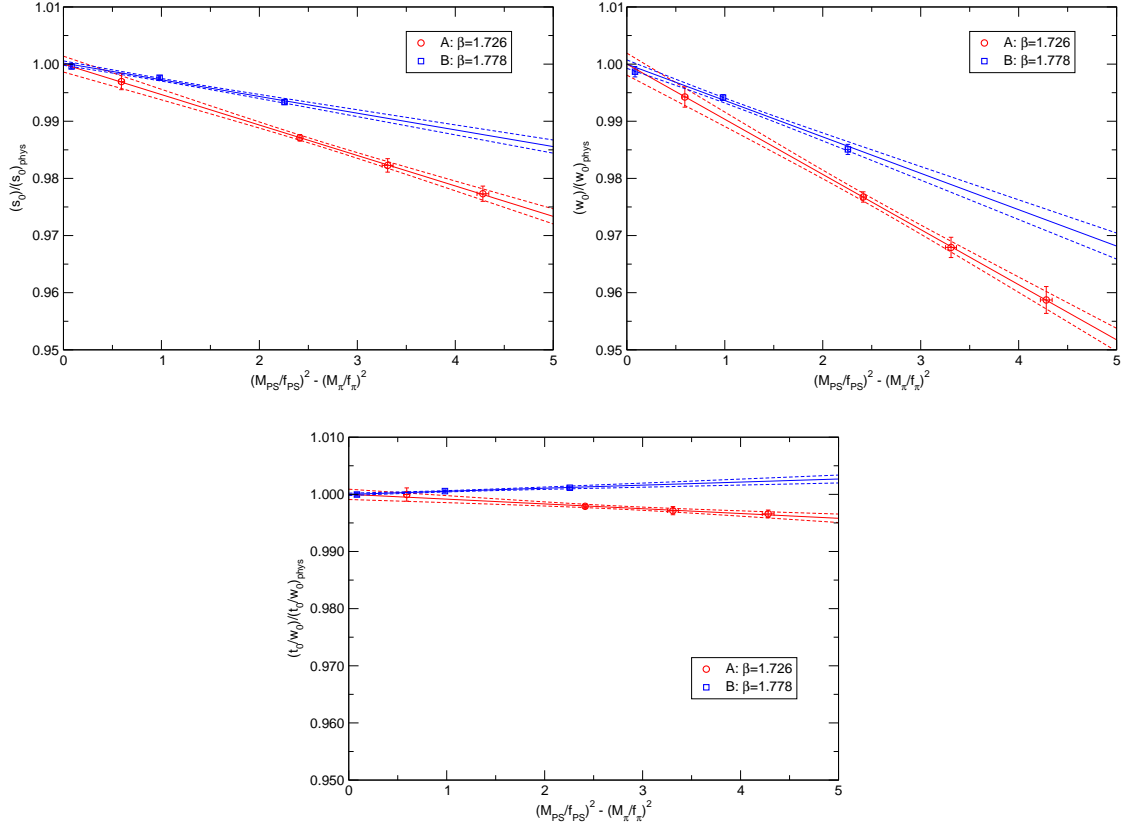


FIG. 10. Light quark-mass dependence and extrapolations to the physical point of the GF scales $s_0 \equiv \sqrt{t_0}$, w_0 , t_0/w_0 , normalised by their values at the physical point for ease of comparing the results at different lattice spacings.

second error reflects the spread of the results while the error in the square bracket is the combined one. These results provide a nontrivial check of the expected scaling behaviour with quantities determined with an accuracy of between 1 - 2 permille for the scales and sub-permille for the ratio, and they nicely confirm the automatic $\mathcal{O}(a)$ -improvement in place for TM Wilson fermions at maximal twist.

Given the fact that the ratio at the physical point shows a very nice $\mathcal{O}(a^2)$ -scaling, we may attempt a global fit in order to extrapolate simultaneously to the physical pion mass and to the continuum limit, using

$$\frac{s_0}{w_0} \left(\frac{M_{\text{PS}}}{f_{\text{PS}}}, \left(\frac{a}{w_0} \right)^2 \right) = \left(\frac{s_0}{w_0} \right)_{\text{cont.}}^{\text{phys.}} + A_1 \cdot \left(\frac{a}{w_0} \right)^2 + (B_0 + B_1 \cdot \frac{a^2}{w_0^2}) \left(\frac{M_{\text{PS}}^2}{f_{\text{PS}}^2} - \frac{M_{\pi}^2}{f_{\pi}^2} \right), \quad (\text{D1})$$

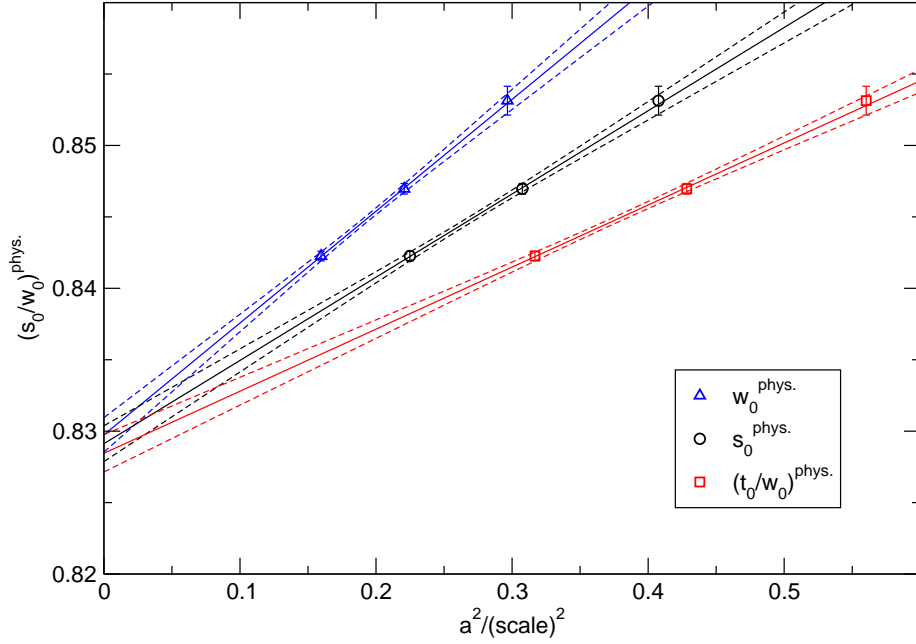


FIG. 11. Continuum extrapolations of the dimensionless ratio of GF scales s_0/w_0 at the physical point in terms of the lattice spacing in units of the GF scales $s_0^{\text{phys.}}$, $w_0^{\text{phys.}}$ and $t_0^{\text{phys.}}/w_0^{\text{phys.}}$ at the physical point.

which includes a light quark-mass dependence proportional to Δ^2 described by B_0 and lattice artefacts proportional to a^2/w_0^2 described by A_1 and B_1 . The latter coefficient describes the lattice artefacts on the quark-mass dependence. The global fit suggests that B_0 , describing the quark-mass dependence in the continuum, is well consistent with zero, i.e., $B_0 = 0.001(7)$. That is, in the continuum the ratio $\sqrt{t_0}/w_0$ appears to have no dependence on the pion mass at all and the observed pion-mass dependence at finite lattice spacings is apparently just a lattice artefact. However, given the fact that we do not have data for the ratio at the lattice spacing cC211 away from the physical point, and hence no information on the quark-mass dependence at the finest lattice spacing, it is not clear how solid this conclusion is. Nevertheless, we may attempt to fit our data with $B_0 = 0$ fixed, and in figure 12 we show the results for this global fit. The coloured lines with error bands show the light quark-mass dependence of the ratio and the extrapolations to the physical point for each lattice spacing, while the black line with

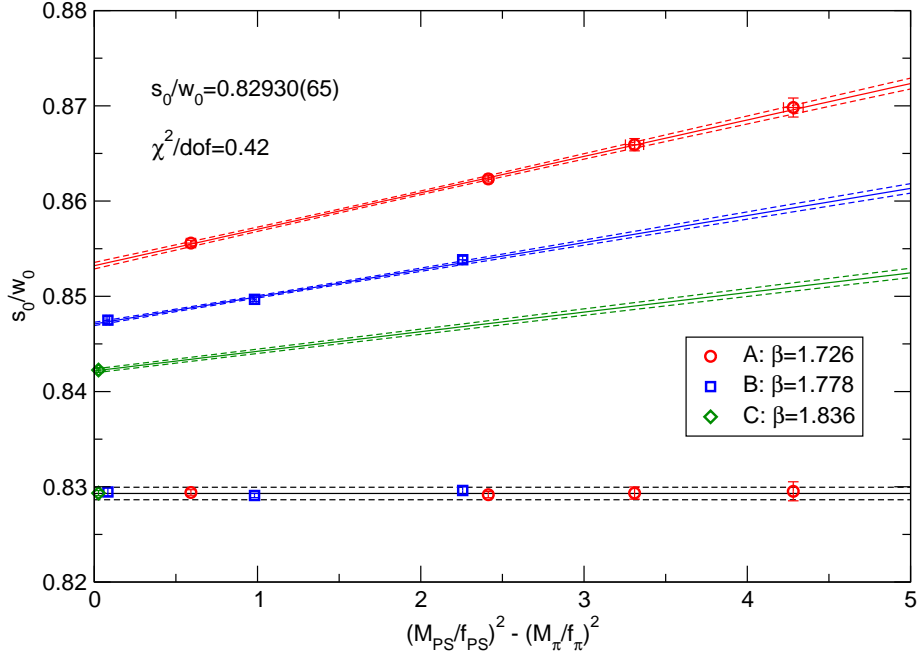


FIG. 12. Global fit of the lattice spacing and light quark-mass dependence of the dimensionless ratio $s_0/w_0 \equiv \sqrt{t_0}/w_0$. The black line with the error band at the bottom shows the fit result in the continuum, while the data points on this line represent the data corrected by the lattice artefacts as described by the global fit.

the error band at the bottom shows the fit result in the continuum. The data points on this line represent our data corrected by the lattice artefacts as described by the global fit.

For the ratio at the physical point and in the continuum the fit yields

$$\left(\frac{s_0}{w_0}\right)_{\text{cont.}}^{\text{phys.}} = 0.82930(65) \quad (\text{D2})$$

with $\chi^2/d.o.f. = 0.42$, $N_{d.o.f.} = 5$ and $A_1 = 0.0806(30)$, $B_1 = 0.0129(5)$.

We note that the ratio is determined with a precision in the sub-permille region, i.e., better than 0.8 permille. As such, it provides an interesting consistency crosscheck on any other, independent determination of the scales, e.g., through hadronic quantities.

2. Determination of the GF scales $\sqrt{t_0}$ and t_0/w_0

The SU(2) ChPT analysis of the data for X_π , carried out in Section IV B adopting the GF scale w_0 , can be repeated in the case of the scales $\sqrt{t_0}$ and t_0/w_0 . The values of the relative GF scales w_0/a , $\sqrt{t_0}/a$ and $t_0/(w_0a)$ have been calculated at the physical pion point in the previous Section D 1 and, for sake of clarity, we recollect them in Table X.

β	w_0/a	$\sqrt{t_0}/a$	$t_0/(w_0a)$
1.726	1.8352 (35)	1.5660 (22)	1.3359 (12)
1.778	2.1299 (16)	1.80396 (68)	1.52789 (33)
1.836	2.5045 (17)	2.1094 (8)	1.77670 (37)

TABLE X. Values of the relative GF scales w_0/a , $\sqrt{t_0}/a$ and $w_0/(w_0a)$ obtained at the physical pion point in Section D 1.

Adopting fitting functions similar to the ones given by Eq. (56) used in the case of the scale w_0 , we obtain

$$w_0 = 0.17383 (57)_{\text{stat+fit}} (26)_{\text{syst}} [63] \text{ fm} , \quad (\text{D3})$$

$$\sqrt{t_0} = 0.14436 (54)_{\text{stat+fit}} (30)_{\text{syst}} [61] \text{ fm} , \quad (\text{D4})$$

$$\frac{t_0}{w_0} = 0.11969 (52)_{\text{stat+fit}} (33)_{\text{syst}} [62] \text{ fm} . \quad (\text{D5})$$

The quality of the fitting procedure in the case of the GF scales $\sqrt{t_0}$ and t_0/w_0 is illustrated in Fig. 13 and it should be compared with the one shown in Fig. 6 in the case of the GF scale w_0 .

Some values obtained for the continuum-limit fitting parameters f and $\bar{\ell}_4^{\text{phys}}$ and for the discretization parameters D'_0 and D'_1 are collected in Table XI. It can clearly be seen that the pion mass dependence of X_π in the continuum limit is stable against the choice of the specific GF scale, while the values of the discretization parameters D'_0 and D'_1 depend on the above choice. The discretization effects on X_π appear to be smaller in the case of the GF scale t_0/w_0 .

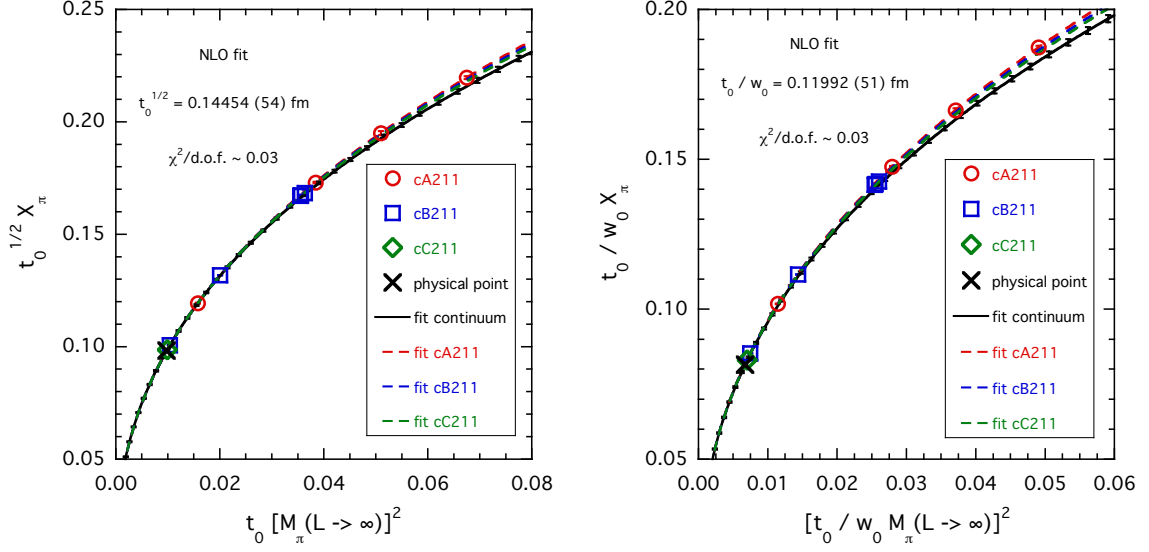


FIG. 13. *The same as in Fig. 6, but in the case of the GF scales $\sqrt{t_0}$ (left panel) and t_0/w_0 (right panel).*

GF scale	f (MeV)	$\bar{\ell}_4^{phys}$	D'_0	D'_1
w_0	124.4 (1.2)	3.24 (29)	-0.167 (52)	8.0 (2.3)
$\sqrt{t_0}$	124.5 (1.2)	3.16 (27)	-0.065 (40)	6.3 (1.6)
t_0/w_0	124.7 (1.3)	3.08 (27)	-0.003 (32)	4.9 (1.2)

TABLE XI. *Values of the fitting parameters f and $\bar{\ell}_4^{phys}$ and of the discretization parameters D'_0 and D'_1 obtained in the case of the three GF scales w_0 , $\sqrt{t_0}$ and t_0/w_0 using the data on X_π and adopting fitting functions similar to Eq. (56) with $A'_2 = F_{FVE} = 0$.*

Finally, the values of the lattice spacing a corresponding to the three GF scales (D3-D5) and to the relative scales given in Table X are shown in Table XII. The three determinations of a differ by $\mathcal{O}(a^2)$ effects, as shown in Fig. 14. In particular, we get: $a(\sqrt{t_0})/a(w_0) \simeq 1 - 0.09(2) a^2(w_0)/w_0^2$ and $a(t_0/w_0)/a(w_0) \simeq 1 - 0.18(2) a^2(w_0)/w_0^2$.

[1] N. Cabibbo, *Phys. Rev. Lett.* **10**, 531 (1963).

GF scale	$a(\beta = 1.726)$ (fm)	$a(\beta = 1.778)$ (fm)	$a(\beta = 1.836)$ (fm)
w_0	0.09471 (39)	0.08161 (30)	0.06941 (26)
$\sqrt{t_0}$	0.09217 (41)	0.08002 (34)	0.06844 (29)
t_0/w_0	0.08960 (47)	0.07834 (41)	0.06737 (35)

TABLE XII. Values of the lattice spacing a corresponding to the three GF scales w_0 , $\sqrt{t_0}$, t_0/w_0 and to the corresponding relative scales given in Table X.

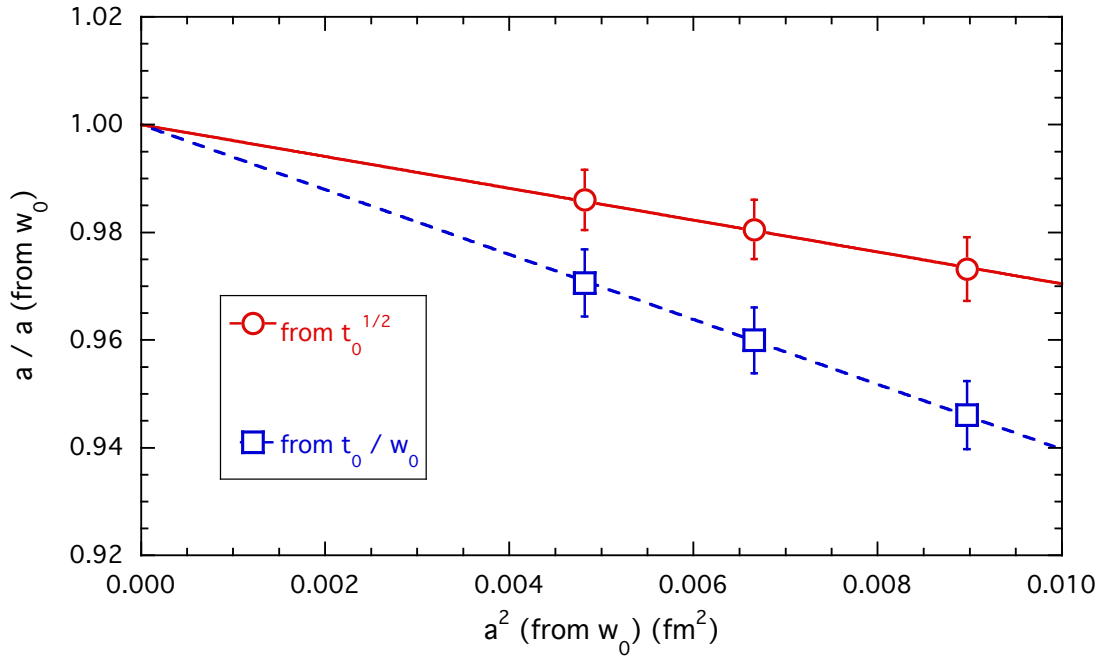


FIG. 14. Ratio of the lattice spacing a obtained from the GF scales $\sqrt{t_0}$ (red circles) and t_0/w_0 (blue squares) with the one determined from the GF scale w_0 (see Table XII). The solid and dashed lines are linear fits.

- [2] M. Kobayashi and T. Maskawa, *Prog. Theor. Phys.* **49**, 652 (1973).
- [3] P. A. Zyla *et al.* (Particle Data Group), *PTEP* **2020**, 083C01 (2020).
- [4] D. Giusti, V. Lubicz, G. Martinelli, C. T. Sachrajda, F. Sanfilippo, S. Simula, N. Tantalo, and C. Tarantino, *Phys. Rev. Lett.* **120**, 072001 (2018), arXiv:1711.06537 [hep-lat].
- [5] M. Di Carlo, D. Giusti, V. Lubicz, G. Martinelli, C. T. Sachrajda, F. Sanfilippo, S. Simula, and N. Tantalo, *Phys. Rev. D* **100**, 034514 (2019), arXiv:1904.08731 [hep-lat].

- [6] J. Gasser and G. R. S. Zarnauskas, *Phys. Lett. B* **693**, 122 (2010), [arXiv:1008.3479 \[hep-ph\]](#).
- [7] S. Aoki *et al.*, *Eur. Phys. J. C* **77**, 112 (2017), [arXiv:1607.00299 \[hep-lat\]](#).
- [8] C. Patrignani *et al.* (Particle Data Group), *Chin. Phys. C* **40**, 100001 (2016).
- [9] J. Hardy and I. S. Towner, *PoS CKM2016*, 028 (2016).
- [10] J. Gasser, A. Rusetsky, and I. Scimemi, *Eur. Phys. J. C* **32**, 97 (2003), [arXiv:hep-ph/0305260](#).
- [11] C. Alexandrou *et al.*, *Phys. Rev. D* **98**, 054518 (2018), [arXiv:1807.00495 \[hep-lat\]](#).
- [12] G. Bergner, P. Dimopoulos, J. Finkenrath, E. Fiorenza, R. Frezzotti, M. Garofalo, B. Kostrzewa, F. Sanfilippo, S. Simula, and U. Wenger (Extended Twisted Mass), *PoS LATTICE2019*, 181 (2020), [arXiv:2001.09116 \[hep-lat\]](#).
- [13] S. Borsanyi *et al.*, *JHEP* **09**, 010 (2012), [arXiv:1203.4469 \[hep-lat\]](#).
- [14] M. Lüscher, *JHEP* **08**, 071 (2010), [Erratum: *JHEP* 03, 092 (2014)], [arXiv:1006.4518 \[hep-lat\]](#).
- [15] A. Bazavov *et al.* (MILC), *Phys. Rev. D* **93**, 094510 (2016), [arXiv:1503.02769 \[hep-lat\]](#).
- [16] R. J. Dowdall, C. T. H. Davies, G. P. Lepage, and C. McNeile, *Phys. Rev. D* **88**, 074504 (2013), [arXiv:1303.1670 \[hep-lat\]](#).
- [17] S. Borsanyi *et al.*, *Nature* **593**, 51 (2021), [arXiv:2002.12347 \[hep-lat\]](#).
- [18] N. Miller *et al.*, *Phys. Rev. D* **103**, 054511 (2021), [arXiv:2011.12166 \[hep-lat\]](#).
- [19] S. Aoki *et al.* (Flavour Lattice Averaging Group), *Eur. Phys. J. C* **80**, 113 (2020), [arXiv:1902.08191 \[hep-lat\]](#).
- [20] N. Carrasco *et al.*, *Phys. Rev. D* **91**, 054507 (2015), [arXiv:1411.7908 \[hep-lat\]](#).
- [21] A. Bazavov *et al.*, *Phys. Rev. D* **98**, 074512 (2018), [arXiv:1712.09262 \[hep-lat\]](#).
- [22] C.-Y. Seng, M. Gorchtein, H. H. Patel, and M. J. Ramsey-Musolf, *Phys. Rev. Lett.* **121**, 241804 (2018), [arXiv:1807.10197 \[hep-ph\]](#).
- [23] S. Romiti and S. Simula, *Phys. Rev. D* **100**, 054515 (2019), [arXiv:1907.09926 \[hep-lat\]](#).
- [24] G. Colangelo, S. Durr, and C. Haefeli, *Nucl. Phys. B* **721**, 136 (2005), [arXiv:hep-lat/0503014](#).
- [25] Y. Iwasaki, *Nucl. Phys. B* **258**, 141 (1985).
- [26] B. Sheikholeslami and R. Wohlert, *Nucl. Phys. B* **259**, 572 (1985).
- [27] S. Aoki, R. Frezzotti, and P. Weisz, *Nucl. Phys. B* **540**, 501 (1999), [arXiv:hep-lat/9808007](#).
- [28] R. Frezzotti and G. C. Rossi, *JHEP* **08**, 007 (2004), [arXiv:hep-lat/0306014](#).
- [29] R. Frezzotti, G. Martinelli, M. Papinutto, and G. C. Rossi, *JHEP* **04**, 038 (2006), [arXiv:hep-lat/0503034](#).

- [30] K. Osterwalder and E. Seiler, *Annals Phys.* **110**, 440 (1978).
- [31] R. Frezzotti and G. C. Rossi, *JHEP* **10**, 070 (2004), [arXiv:hep-lat/0407002](#).
- [32] R. Frezzotti, P. A. Grassi, S. Sint, and P. Weisz (Alpha), *JHEP* **08**, 058 (2001), [arXiv:hep-lat/0101001](#).
- [33] C. McNeile and C. Michael (UKQCD), *Phys. Rev. D* **73**, 074506 (2006), [arXiv:hep-lat/0603007](#).
- [34] J. Gasser and H. Leutwyler, *Annals Phys.* **158**, 142 (1984).
- [35] R. Frezzotti, V. Lubicz, and S. Simula (ETM), *Phys. Rev. D* **79**, 074506 (2009), [arXiv:0812.4042 \[hep-lat\]](#).
- [36] N. Miller *et al.*, *Phys. Rev. D* **102**, 034507 (2020), [arXiv:2005.04795 \[hep-lat\]](#).
- [37] M. Moulson, *PoS CKM2016*, 033 (2017), [arXiv:1704.04104 \[hep-ex\]](#).
- [38] N. Carrasco, P. Lami, V. Lubicz, L. Riggio, S. Simula, and C. Tarantino, *Phys. Rev. D* **93**, 114512 (2016), [arXiv:1602.04113 \[hep-lat\]](#).
- [39] Jülich Supercomputing Centre, *Journal of large-scale research facilities* **A132** (2018), [doi:10.17815/jlsrf-4-121-1](#).
- [40] Jülich Supercomputing Centre, *Journal of large-scale research facilities* **A135** (2019), [doi:10.17815/jlsrf-5-171](#).
- [41] T. Chiarappa, F. Farchioni, K. Jansen, I. Montvay, E. E. Scholz, L. Scorzato, T. Sudmann, and C. Urbach, *Eur. Phys. J. C* **50**, 373 (2007), [arXiv:hep-lat/0606011](#).
- [42] A. D. Kennedy, I. Horvath, and S. Sint, *Nucl. Phys. B Proc. Suppl.* **73**, 834 (1999), [arXiv:hep-lat/9809092](#).
- [43] M. A. Clark and A. D. Kennedy, *Phys. Rev. Lett.* **98**, 051601 (2007), [arXiv:hep-lat/0608015](#).
- [44] M. Luscher, in *Les Houches Summer School: Session 93: Modern perspectives in lattice QCD: Quantum field theory and high performance computing* (2010) [arXiv:1002.4232 \[hep-lat\]](#).
- [45] E. I. Zolotarev, *Zap. Imp. Akad. Nauk. St. Petersburg* **30** (1877).
- [46] I. Omelyan, I. Mryglod, and R. Folk, *Computer Physics Communications* **151**, 272 (2003).
- [47] K. Jansen and C. Urbach, *Comput. Phys. Commun.* **180**, 2717 (2009), [arXiv:0905.3331 \[hep-lat\]](#).
- [48] A. Deuzeman, K. Jansen, B. Kostrzewa, and C. Urbach, *PoS LATTICE2013*, 416 (2014), [arXiv:1311.4521 \[hep-lat\]](#).
- [49] A. Abdel-Rehim, F. Burger, A. Deuzeman, K. Jansen, B. Kostrzewa, L. Scorzato, and C. Urbach, *PoS LATTICE2013*, 414 (2014), [arXiv:1311.5495 \[hep-lat\]](#).

- [50] S. Bacchio, C. Alexandrou, and J. Finkenrath, *EPJ Web Conf.* **175**, 02002 (2018), [arXiv:1710.06198 \[hep-lat\]](#).
- [51] S. Bacchio, C. Alexandrou, J. Finkenrath, A. Frommer, K. Kahl, and M. Rottmann, *PoS LATTICE2016*, 259 (2016), [arXiv:1611.01034 \[hep-lat\]](#).
- [52] C. Alexandrou, S. Bacchio, J. Finkenrath, A. Frommer, K. Kahl, and M. Rottmann, *Phys. Rev. D* **94**, 114509 (2016), [arXiv:1610.02370 \[hep-lat\]](#).
- [53] C. Alexandrou, S. Bacchio, and J. Finkenrath, *Comput. Phys. Commun.* **236**, 51 (2019), [arXiv:1805.09584 \[hep-lat\]](#).
- [54] B. Joó, D. D. Kalamkar, T. Kurth, K. Vaidyanathan, and A. Walden, in *High Performance Computing*, edited by M. Tauber, B. Mohr, and J. M. Kunkel (Springer International Publishing, Cham, 2016) pp. 415–427.
- [55] B. Joó, D. Kalamakar, K. Vaidyanathan, M. Smelyanskiy, T. Kurth, A. Walden, M. Schroeck, P. Labus, M. Ueding, B. Kostrzewa, and D. Dep, <https://github.com/JeffersonLab/qphix>.
- [56] M. Luscher, S. Sint, R. Sommer, and P. Weisz, *Nucl. Phys. B* **478**, 365 (1996), [arXiv:hep-lat/9605038](#).
- [57] R. Frezzotti, S. Sint, and P. Weisz (ALPHA), *JHEP* **07**, 048 (2001), [arXiv:hep-lat/0104014](#).
- [58] M. Luscher and P. Weisz, *JHEP* **02**, 051 (2011), [arXiv:1101.0963 \[hep-th\]](#).
- [59] A. Deuzeman and U. Wenger, *PoS LATTICE2012*, 162 (2012).